Complex ^{40}Ar/^{39}Ar age spectra from low-grade metamorphic ~~grade~~ rocks: resolving the input of detrital and metamorphic components in a case study from the Delamerian Orogen

Anthony Reid[1, 2], Marnie Forster[3], Wolfgang Preiss[1, 2], Alicia Caruso[1], Stacey Curtis[1,4], Tom Wise[1], Davood Vasegh[3], Naina Goswami[3], Gordon Lister[5]

[1]Geological Survey of South Australia, Department of State Development, GPO Box 320, Adelaide, SA 5001, Australia
[2]Department of Earth Sciences, School of Physical Sciences, University of Adelaide, SA 5005, Australia
[3]Mineral Exploration Cooperative Research Centre, Research School of Earth Sciences, The Australian National University, Canberra, ACT 2601, Australia.
[4]Mineral Exploration Cooperative Research Centre, STEM, University of South Australia, Mawson Lakes, Australia
[5]Sustainable Minerals Institute, University of Queensland, Brisbane, Australia

Correspondence to: Anthony Reid (anthony.reid@sa.gov.au)

Abstract. In this study, we provide ^{40}Ar/^{39}Ar geochronology data from a suite of variably deformed rocks from a region of low-grade metamorphism within the Cambro-Ordovician Delamerian Orogen, South Australia. Low-grade metamorphic ~~grade~~ rocks such as these can contain both detrital minerals and minerals newly grown or partly recrystallised during diagenesis and metamorphism. ~~However, rocks such as these~~ Hence, they typically yield complex ^{40}Ar/^{39}Ar age spectra that can be difficult to interpret. ~~In this study~~ Therefore, we have ~~analysed a suite of variably deformed rocks from a region of low metamorphic grade within the c. 514 – 490 Ma Delamerian Orogen, South Australia.~~ undertaken furnace step heating ^{40}Ar/^{39}Ar geochronology to obtain age spectra with many steps, so as to allow application of the method of asymptotes and limits, and recognition of the effects of mixing. The samples analysed range from siltstone and shale to phyllite and ~~all~~ contain ~~either~~ muscovite or phengite with minor microcline as determined by hyperspectral mineralogical characterisation. ~~Furnace step heating ^{40}Ar/^{39}Ar analysis produced complex apparent age spectra with multiple age components. Using the concept of asymptotes that define minimum and maximum~~ Whole rock ^{40}Ar/^{39}Ar analyses were undertaken in most samples due to their very fine-grained nature. All samples are dominated by radiogenic ^{40}Ar, and contain minimal evidence for atmospheric, Ca- or Cl-derived argon. Chloritisation may have resulted in limited recoil causing ^{39}Ar argon loss in some samples, especially evident within the first few percent of gas release. Most of the age data, however, appear to have some geological significance. Viewed with respect to the known depositional ages ~~for different components, we interpret~~ of the stratigraphic units, the age spectra ~~to preserve a range of~~ from this study do appear to record both detrital mineral ages, ~~along with younger components and ages~~ related to the varying influence of either cooling or deformation-induced recrystallisation. ~~Two samples contain Mesoproterozoic detrital age components, up to c. 1170 Ma, while the c. 515 Ma Heatherdale Shale which has both c. 566 Ma and c. 530 Ma detrital components. All samples contain younger lower (younger) asymptotes in the age spectra defined from multiple heating steps that range from c. 476 to c. 460 Ma. One interpretation of these younger ages is that they are caused by~~

~~post-metamorphic cooling. However, the~~The shape of the age spectra and the degree of deformation in the phyllites suggest the younger ages may record recrystallisation of detrital minerals and/or new mica growth during deformation. ~~Potentially~~ ~~these c. 476 to c. 460~~Given that the younger limit of deformation recorded in the high metamorphic grade regions of the Delamerian Orogen is c. 490 Ma, the c. 470 to c. 458 Ma ages obtained in this study suggest deformation in ~~the upper portion~~ ~~of the orogen was~~low-grade shear zones within the Delamerian Orogen may have persisted until c. 20-32 million years after high-temperature ductile deformation in the high-grade regions of the orogen. We suggest these younger ages for deformation could be a result of reactivation of older structures formed both during initial rifting and basin formation and during the main peak of the Delamerian orogeny itself. The younger c. 470 to c. 458 Ma deformation may have been facilitated by ~~movement~~ ~~along regional faults and shear zones up to around 20 million years after the cessation of deformation in the high metamorphic~~ ~~grade regions of the Delamerian Orogen.~~ far-field tectonic processes occurring along the eastern paleo-Pacifc margin of Gondwana.

1 Introduction

~~Low metamorphic grade rocks are a common feature in most orogens as they constitute the upper portion of an orogen, distal~~ ~~to more deeply exhumed high metamorphic grade core. In many orogens, low metamorphic grade~~In many orogens, low-grade metamorphic rocks comprise the vast bulk of the surface exposure, and hence are potentially a significant source of information on the orogenic process. However, most studies into the rates and timing of orogenesis concentrate on the high metamorphic grade sections of orogens largely because high temperature minerals are either completely newly grown during orogenesis, or at least~~,~~ isotopically reset. Low-grade metamorphic ~~grade~~ rocks in contrast~~,~~ typically comprise a mixture of detrital minerals and newly grown diagenetic or metamorphic minerals (e.g. Dallmeyer et al., 1988; Dunlap et al., 1991; Cosca et al., 1992; ~~Kirschner et al., 2003~~Dallmeyer and Takasu, 1992; Chan et al., 2000; Fergusson and Phillips, 2001; ~~Dallmeyer and Takasu,~~ ~~1992; Dallmeyer~~Kirschner et al., ~~1988~~2003; Clauer, 2013). As a result, and especially when dealing with fine-grained, low-metamorphic grade rocks, it can be difficult to separate detrital from metamorphic signals in isotopic analysis of whole rock samples ~~(see also Phillips et al., 2012).~~.

~~In this paper we show that ^{40}Ar/^{39}Ar furnace analysis of low metamorphic grade rocks can provide information on the possible~~ ~~detrital component of these rocks, as well as yield insights into the timing of orogenic activity. This approach can be viewed~~ ~~as complimentary to ^{40}Ar/^{39}Ar dating low metamorphic grade rock fabrics using in situ laser microprobe methods.~~ ^{40}Ar/^{39}Ar geochronology of fine-grained and typically low-grade metamorphic rock samples poses significant methodological challenges, including the problem of inheritance from pre-metamorphic minerals and recoil loss and ^{39}Ar redistribution due to the fine-grained nature of the analysed minerals (~~e.g. Chan~~Fergusson and Phillips, 2001; Phillips et al., ~~2000; Kirkland et al.,~~

65 ~~20082012). Our field area, the Mount Lofty Ranges of South Australia, provides an ideal setting with which to investigate low metamorphic grade rocks, because of the extensive exposure of Neoproterozoic to Cambrian metasedimentary rocks in this part of the Delamerian Orogen. The results identify Mesoproterozoic detrital components along with Cambro-Ordovician age populations related to cooling or deformation.~~

. Inheritance can be a major problem and result in over estimation of deformation ages if the age of detrital and newly grown
70 minerals is either very close in time, or if there are limited heating steps with poor temperature control resulting in averaging of gas from different mineralogical components. One approach to minimising this problem has been to use laser ablation heating and apply this to specific mineral grains either separated manually or analysed in situ (e.g. Chan et al., 2000; Haines et al., 2004; Kirkland et al., 2008). This can work well in the case where detrital minerals are relatively coarse grained, however, the smaller gas portions obtained via laser fusion can affect age precision. Recoil of ^{39}Ar during neutron irradiation can
75 artificially reduce apparent ages and is especially problematic in fine grained samples that have undergone chloritic alteration (Lo and Onstott, 1989). Methodological attempts to minimise ^{39}Ar recoil have been made, such as by encapsulation of samples during irradiation (Foland et al., 1992); however, this method produces a single age per sample and is not appropriate for samples which may have multiple age populations. Therefore, resolving detrital from metamorphic signals in complex age spectra remains a challenging task, with the result that low-grade rocks are often overlooked in studies on the timing of
80 deformation in orogenic belts.

In this paper we show that furnace step heating can yield meaningful age gradients in ^{40}Ar/^{39}Ar age spectra from fine-grained whole rock samples and mica separates. In this respect, we utilise a similar methodology to Dallmeyer et al. (1988) who analysed whole rock slate and phyllite samples via furnace step heating. However, here we apply a careful heating schedule
85 for our ultrahigh vacuum (UHV) step heating experiments, utilising a larger number of increments in the step-heating schedule to carefully resolve any variations in age within the sample (thereby appyling methods similar to Forster and Lister, 2009; Muston et al., 2021).

Our field area, the Delamerian Orogen exposed in the Mount Lofty Ranges of South Australia, provides an ideal setting with
90 which to investigate low-grade metamorphic rocks, because of the extensive exposure of Neoproterozoic to Cambrian metasedimentary units. The timing of orogenic activity in the Delamerian Orogen has been established based on cross-cutting relationships of igneous rocks from high-grade metamorphic zones of the orogen. The earliest interpreted syn-tectonic intrusion within the orogen has a U-Pb zircon age of 514 ± 4 Ma (Rathjen Gneiss; Foden et al., 1999). Bimodal intrusions that cut tectonic fabrics and are weakly or undeformed themselves were emplaced between c. 490 and 470 Ma. While the ages of these
95 magmatic rocks are interpreted to bracket the timing of deformation between c. 514 – 490 Ma (Foden et al., 2020), there has been little geochronology from low-grade portions of the orogen to determine if deformation was synchronous across metamorphic grade zones. Our new samples yield complex age spectra that we interpret to contain evidence for ages from

detrital minerals up to Mesoproterozoic in age, as well as ages from newly grown minerals of Cambro-Ordovician age related to cooling and/or deformation.

100 2 Geological setting

The Delamerian Orogen formed on the eastern proto-Pacifc margin of Gondwana in the Late Cambrian to early Ordovician and is part of the family of orogens developed during amalgamation of Gondwana (Fig. 1; Preiss, 1995; 1995a; Cawood, 2005; Foden et al., 2006; Cawood, 2005; Glen and Cooper, 2021). The Delamerian Orogeny deformed Neoproterozoic to early Cambrian rocks of the Adelaide Superbasin, including the early Cambrian Kanmantoo Group and Normanville Groups. The

105 Neoproterozoic stratigraphy includes the Burra, Umberatana and Wilpena Groups, which were deposited in a series of rift and sag basins associated with the breakup of the supercontinent Rodinia (Fig. 2; Preiss, 2000; Lloyd et al., 20201987; Preiss, 1995a; Flottmann et al., 1998; Preiss, 19872000; Lloyd et al., 2020). Deposition of the Kanmantoo and Normanville groups iswas contemporaneous with the earliest arc magmatism along the Gondwanan subduction margin to the east of the Delamerian Orogen (Betts et al., 2018). The Delamerian Orogen is a fold-thrust belt in which the rift complex units, as well as parts of the

110 underlying Paleo-Mesoproterozoic basement, were thrust towards the Archean-Mesoproterozoic Gawler Craton. A series of western frontal thrusts separate the strongly folded and faulted rocks from the Torrens Hinge Zone, a zone of transition between the thick, highly deformed succession and the platform sediments of the Stuart Shelf that overlie the basement of the Gawler Craton to the west (Fig. 3; e.g. Flottmann and James, 1997). There is no compelling evidence of deformation, other than rifting, between the Neoproterozoic and Cambrian, and both successions have been deformed and metamorphosed together.

115 Metamorphic isograds cross some stratigraphic boundaries, especially within the Kanmantoo Group, but some others coincide with major faults (Fig. 3; Offler and Fleming, 1968; Mancktelow, 1990; Dymoke and Sandiford, 1992). The lowest metamorphic grade regions occur along the western edge of the orogen, where weakly cleaved rocks contain metamorphic chlorite defining a chlorite-zone (Fig. 3), from where several samples analysed in this study were derived. Peak metamorphic conditions of ~3-5 kbar and 550-650 °C occur in a migmatite-grade zone in the east of the orogen, demonstrating regional

120 metamorphism low-pressure, medium- to high-temperature in style (Dymoke and Sandiford, 1992; Preiss, 1995).(Betts et al., 2018; Cayley and Skladzien, 2018). Deformation and metamorphism began at c. 514 Ma with emplacement of early, syn-tectonic granite (Foden et al., 1999). A belt of, high-level, undeformed granites cut major structures in the eastern parts of the orogen formed at c. 490 Ma, suggesting that the entire orogenic cycle occurred over an approximately ~24 million year period in the late Cambrian (Foden et al., 2006).

125

Peak metamorphic conditions of ~3-5 kbar and 550-650 °C occur in a migmatite-grade zone in the east of the orogen (Dymoke and Sandiford, 1992; Preiss, 1995a). Metamorphic isograds for the Delamerian Orogen cross some stratigraphic boundaries and folds especially within the Kanmantoo Group, supporting the notion that metamorphism was both synchronous with but also overprints some of the large-scale deformation features (Fig. 2; Offler and Fleming, 1968; Mancktelow, 1990; Dymoke

130 and Sandiford, 1992). Folding in the orogen was also synchronous with thrusting, with thrust zones in the western region of the Delamerian displaying fault-bend folding in the hangingwall (Fig. 3; Preiss, 1995a; Flottmann and James, 1997; Flottmann et al., 1998; Preiss, 2019). The lowest metamorphic grade regions occur along the western edge of the orogen, where weakly cleaved rocks as well as phyllitic shear zones contain metamorphic chlorite, thereby defining a chlorite-zone (Fig. 2), from where several samples analysed in this study were derived.

135

The few available ^{40}Ar/^{39}Ar analyses from the Delamerian Orogen have mostly been interpreted to record post-peak metamorphic cooling (FodenTurner et al., 20201996; Foden et al., 2006; Turner et al., 19962009; Foden et al., 2020). Laser induced step heating ^{40}Ar/^{39}Ar analyses of syn-kinematic muscovite from folded schists in the Delamerian Orogen yielded a plateau age of 502 ± 4 Ma, interpreted to record cooling subsequent to D$_1$ thrusting (Foden et al., 2020). Laser ^{40}Ar/^{39}Ar

140 analyses of biotite and hornblende from syn-kinematic, largely I-type granites and fromcountry rocks yield ages that range from c. 498 – 480 Ma (Turner et al., 1996), which broadly corresponds to the timing of intrusion of late-kinematic to post-kinematic granites and mafic rocks. Turner et al. (1996) interpreted the orogen to have cooled below ~300 °C by c. 480 Ma. This is consistent with a muscovite ^{40}Ar/^{39}Ar age of 478 ± 2 Ma from a high-level post-tectonic pegmatite (Burtt and Phillips, 2003). Importantly, however, the currently available ^{40}Ar/^{39}Ar data are all from rocks within the high metamorphic grade

145 portions of the orogen. There is no ^{40}Ar/^{39}Ar data published from the lower metamorphic grade regions of the Delamerian Orogen.

In contrast to these data from the high metamorphic grade portions of the orogen, two studies have used ^{40}Ar/^{39}Ar methods to date low grade rocks from the south-western region of the orogen. Haines et al. (2004) and Turner et al. (2009) present laser

150 fusion ^{40}Ar/^{39}Ar data on detrital muscovite from the Delamerian Orogen. Their results show that many of the Neoproterozoic sedimentary rocks within the Delamerian Orogen contain detrital mica that has preserved signature of the source region and has escaped recrystallisation during orogenic activity. Turner et al. (2009) also dated white mica from a sandstone containing a differentiated cleavage and reported an ^{40}Ar/^{39}Ar age of 533 ± 15 Ma and a Rb/Sr isochron age of 554 ± 10 Ma, which they interpreted to date the timing of cleavage formation at that locality.

155
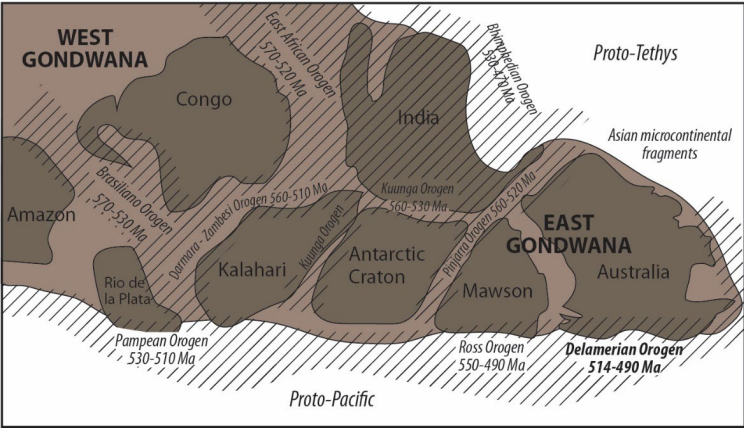
Figure 1. Location of the Delamerian Orogen with respect to east Gondwanan terranes and Pan-African orogens. Modified from Cawood et al. (2007).
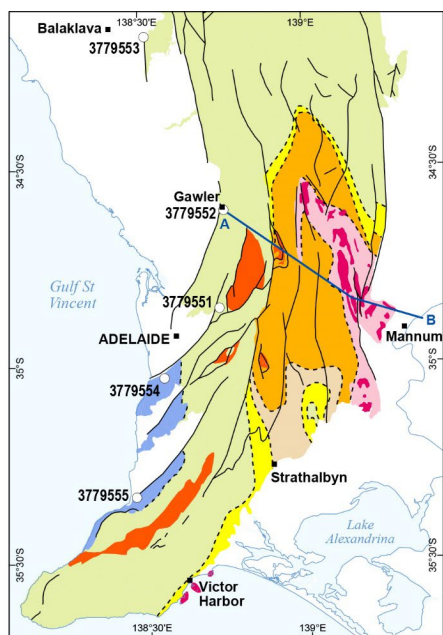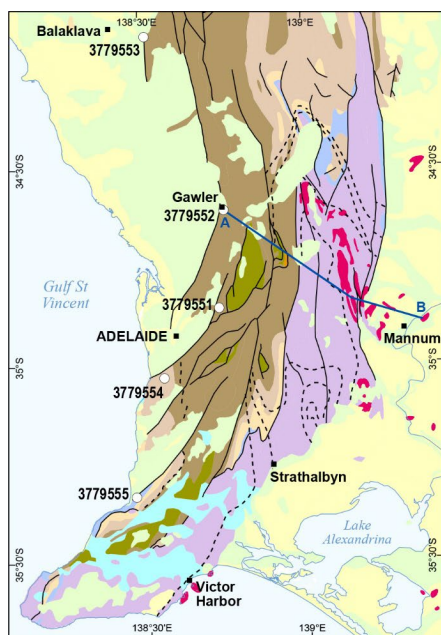
2 000 000 surface geology

CENOZOIC
- Pleistocene–Holocene
- Palaeogene–Neogene

CARBONIFEROUS-PERMIAN
- Cape Jervis Formation

CAMBRIAN-ORDOVICIAN
- Granitoid rock of the Delamerian Orogeny

CAMBRIAN
- Kanmantoo Group
- Normanville Group

NEOPROTEROZOIC
- Wilpena Group
- Umberatana Group
- Burra Group
- Mount Crawford Granite Gneiss

PALAEOPROTEROZOIC
- Barossa Complex

Delamerian metamorphic zones
- Chlorite zone
- Biotite zone
- Barossa Complex amphibolite facies, retrogressed to greenschist facies
- Andalusite-straurolite zone
- Fibrolite zone
- Prismatic sillmanite zone
- Migmatite zone
- Delamerian granite

- Sample locations
- Location of Gawler-Mannum cross-section of Figure 3
- Fault position accurate
- Metamorphic isograd (non-faulted)

DEM 205463-057

0   25   50 Kilometers
GDA2020 Zone 54

160
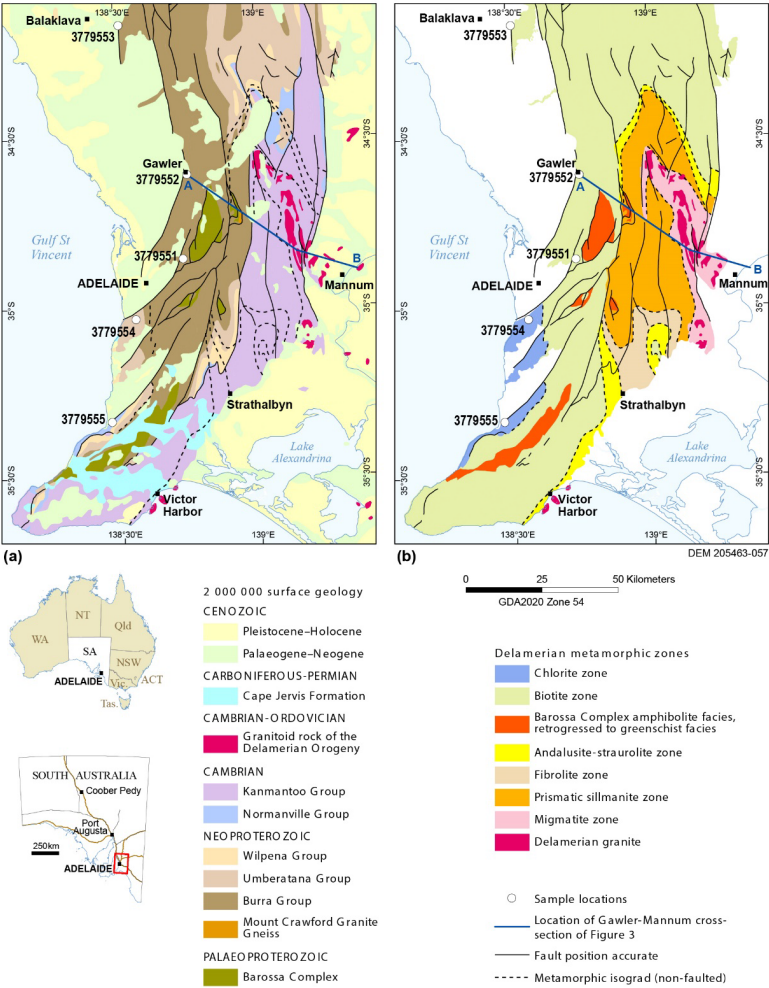
Figure 2: Geology of the Mt Lofty Ranges, part of the Delamerian Orogen, showing location of samples analysed in this study. (a) 1:2 million scale South Australian state-wide geology dataset. (b) Delamerian metamorphic isograds of the Mt Lofty Ranges (after Offler and Fleming, 1968; Mancktelow, 1990; Dymoke and Sandiford, 1992; Preiss, ~~1995~~1995a).
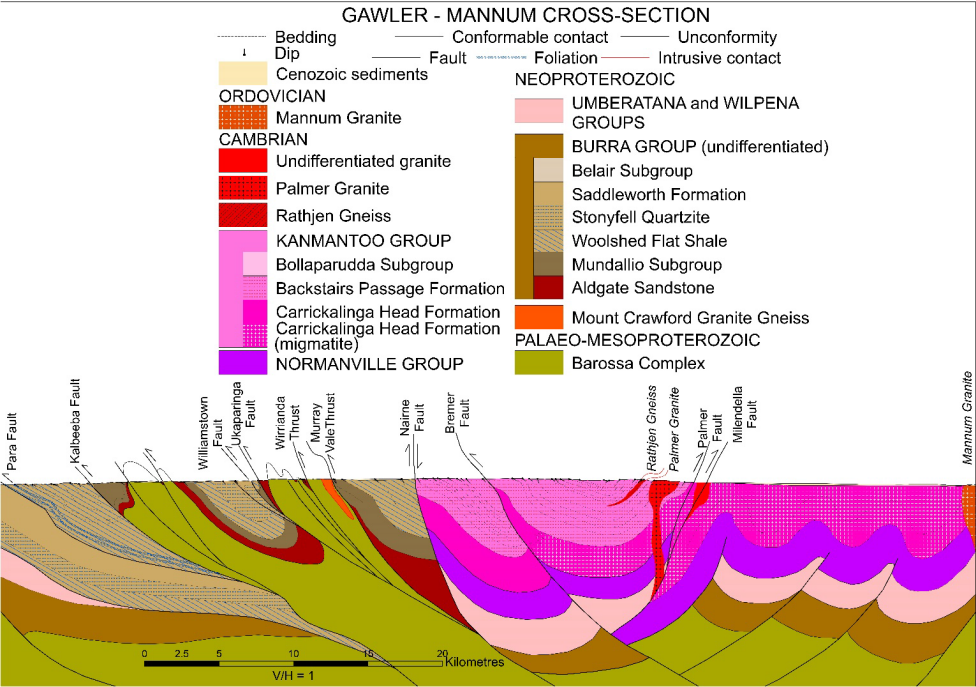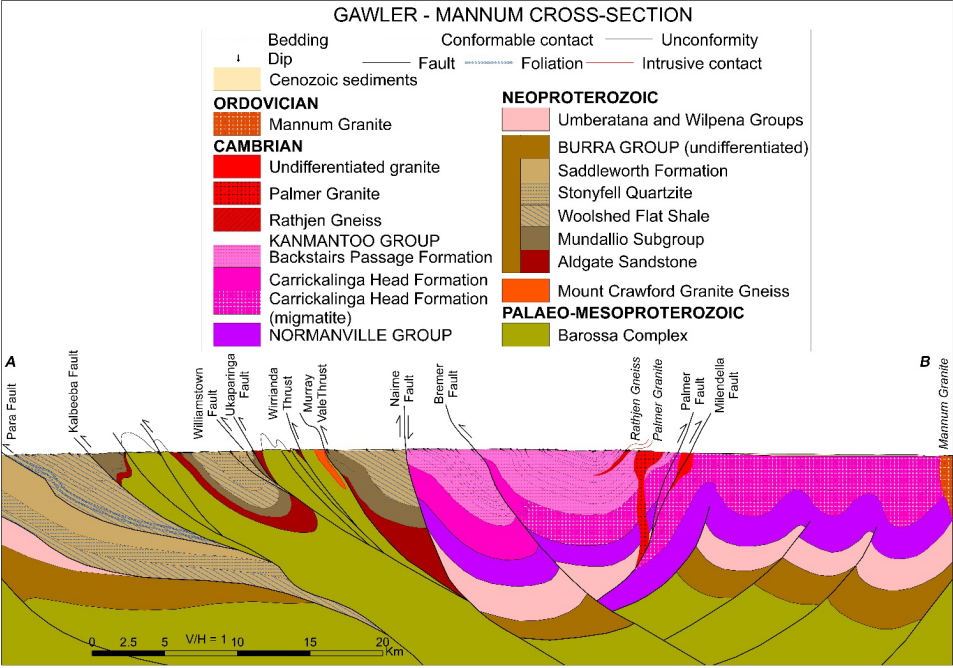
Figure 3. Interpretative cross-section across the southern Delamerian Orogen from Gawler to Mannum. Topographic profile and surface geology, including dip of structural elements, are well constrained from previous mapping, but their extrapolation at depth in this diagram is more speculative. The left-hand portion of the cross-section illustrates the westerly vergence of the major structures in the western, low-grade metamorphic grade zones, and the involvement of the basement. Many of the faults originated as extensional faults in the basement as a result of Neoproterozoic and Cambrian rifting. Of the mapped major faults, the Para, Kalbeeba. Williamstown, Bremer, Palmer and Milendella faults all display compressional neotectonic reactivation. The Nairne Fault differs from other faults in being a ?late Delamerian normal reactivation of a Cambrian extensional fault, and locally forms the western boundary of the Kanmantoo Trough. Metamorphic grade jumps from greenschist facies to sillimanite grade across the Williamstown Fault, while migmatite is widely developed in the oldest formation of the Kanmantoo Group. Geology beneath the Kanmantoo Group is schematic only. Location of cross section shown in Figure 2, A-B.

3 Sample descriptions

To test if the Delamerian Orogen did end at c. 480 Ma across the entire region, weWe have sampled rocks within the biotite and chlorite metamorphic zones of the orogen Delamerian Orogen and analysed them using whole rock ^{40}Ar/^{39}Ar methods (Table 1; Fig. 2). Sample details, including stratigraphic unit and location are given in Table 1. As many of these samples are very fine-grained we have undertaken mineralogical characterization using hyperspectral imaging with Hylogger HyLogger-3™ instrumentation (Schodlok et al., 2016) at the South Australian Drill Core Reference Library, Adelaide. Full details of Hylogger HyLogger-3™ methodology and mineralogical composition of samples from this study are given in Appendix A.

SampleSamples 3779553 is a phyllite in the lower part of the Burra Group, 3779552 and 3779551 are phyllitic schists within low angle thrust zones exposed east of the township of Balaklava. At this locality, the phyllite is a deformed thrust sheet with a low-angle tectonic foliation that sits in the hanging wall of a regional fault (Redbanks Fault).along the western margin of the Mt Lofty Ranges (Figs 2, 4a, b, c). The foliation dips west at a very shallow angle suggesting that it has been gently folded in a hanging-wall antiform (Preiss, 2019). A down-dip mineral lineation is overprinted by mm-scale crenulations trending ~340° (Fig. 4a). This locality is near the western-most extent of the Delamerian Orogen. Mineralogically this sample comprises samples are composed of chlorite (FeMg- and Mg-rich),, phengitic white mica, albite, muscovite and quartz identified across both the Shortwave Infrared (SWIR) and Thermal Infrared (TIR) wavelength ranges, with minor carbonate in sample 3779551 (Appendix A).

Sample 3779552 is a phyllitic schist from within an east-dipping thrust sheet located stratigraphically within the Woolshed Flat Shale, at the southern outskirts of the township of Gawler. The sample is phyllitic, fine-grained, with intense schistosity, and has a well-developed, down-dip mineral lineation (Fig. 4b). The locality also has evidence for boudinaged quartz veins sub-parallel to the foliation, and local mm- to cm-scale quartz veins that cut the foliation. Interpreted SWIR mineralogy for this sample is dominated by chlorite (Fe-Mg-rich) with lesser white mica (phengitic; Appendix A). TIR data shows predominantly quartz and albite (Appendix A).

Sample 3779551, a phyllite, is part of a multiply deformed a high-strain zone within the Woolshed Flat Shale in Torren Gorge, 14 km east-north-east of Adelaide. Two samples were analysed by the ^{40}Ar/^{39}Ar method from this locality. In the nearby Black Hill Conservation Park, a similar phyllite lies in the hanging wall of an east-dipping thrust that places Woolshed Flat Shale over the stratigraphically younger Stonyfell Quartzite. The latter phyllite has a down-dip mineral lineation and a mm-scale crenulation that trends towards ~340° (Fig. 4c). Within this thrust, the phyllite locally contains rafts of dismembered quartzite, which may represent either tectonic slices of Stonyfell Quartzite or sandy interlayers within the Woolshed Flat Shale protolith. Locally, the shear foliation is refolded with secondary open to tight folds, many of which have an axial-planar, spaced

215 ~~crenulation cleavage (Fig. 4d). Mineralogically the samples comprise phengite and chlorite (Fe-Mg-rich), as well as biotite, carbonates, quartz and albite (Appendix A).~~

~~Sample~~ Samples 3779554 ~~is a grey metasiltstone, typical of well laminated~~and 3779555 are siltstones ~~of~~from the Tapley Hill

Formation ~~(depositional age 643.0 ± 2.4 Ma, Re-Os; Kendall et al., 2006), and possessing~~and Heatherdale Shale respectively

220 (Figs 2, 4d, e). Sample 3779554 possesses an upright, slaty cleavage ~~(Fig. 4e)~~. SWIR analysis suggests that the rock ~~comprises~~and is composed of phengitic white mica, ~~while the TIR analysis confirms the presence of~~ quartz, microcline, albite, muscovite and carbonate with minor biotite and phengite (Appendix A).

~~Sample 3779555, from the early Cambrian Heatherdale Shale at the top of the Normanville Group at Sellick Hill, is the~~

225 ~~youngest sample in this study. This locality also lies within the chlorite-grade metamorphic zone (Fig. 2). The sample is a fine-grained siltstone that is moderately fractured, being in the hanging wall of the Willunga Fault (Fig. 3), but does not split readily on its slaty cleavage (Fig. 4f). SWIR analysis suggests sample 3779555 comprises phengite and~~ Sample 3779555 is very weakly cleaved and composed of phengite, kaolinite, ~~while TIR analysis also shows~~ quartz, microcline, muscovite and albite are present (Appendix A). ~~Note that our sample 3779555 was taken very near to a thin layer of ashfall tuff that has been dated~~

230 ~~at 514.98 ± 0.22 Ma (zircon U-Pb, chemical abrasion-thermal ionisation mass spectrometry; Betts et al., 2018).~~ (Appendix A).

Table 1. Details of samples analysed in this study, listed in stratigraphic order.

235 ~~**Table 1.** Sample details.~~

Sample	Rock type	Stratigraphic unit	Depositional age	Location	Easting	Northing	Zone (GDA94)
3779555	siltstone	Heatherdale Shale, Normanville Group	~~515 Ma~~514.98 ± 0.22 Ma (Betts et al., 2018)	Sellick Hill	269649	6086543	54
3779554	siltstone	Tapley Hill Formation, Umberatana Group	~~643.0 ± 2.4 Ma~~643.0 ± 2.4 Ma (Kendall et al., 2006)	Tapley Hill	277441	6120235	54
3779551	phyllite	Woolshed Flat Shale, Burra Group	~~700-800~~790 – 730 Ma (Preiss, 2000; Lloyd et al., 2020)	Torrens Gorge	292907	6140205	54
3779552	phyllite	Woolshed Flat Shale, Burra Group	~~700-800~~790 – 730 Ma (Preiss, 2000; Lloyd et al., 2020)	Deadmans Pass	294054	6167780	54
3779553	phyllite	Undifferentiated Burra Group	~~700-~~800 – 730 Ma (Preiss, 2000; Lloyd et al., 2020)	The Rocks	271453	6216509	54
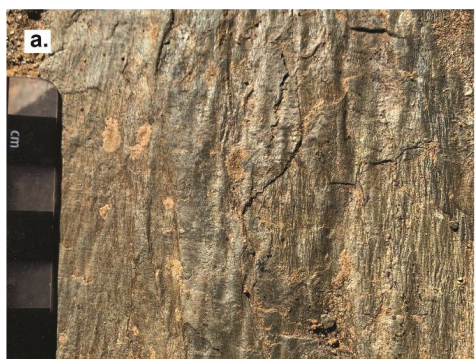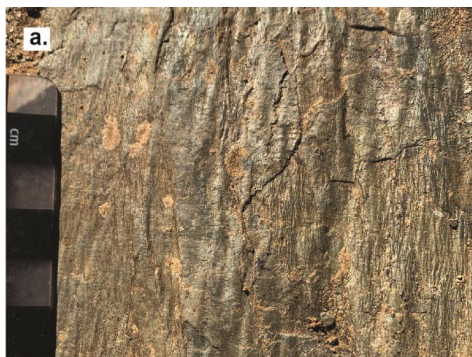
Figure 4: Field photographs of analysed samples. a. Surface of shear fabric in phyllite from the locality of sample 3779553. b. Cross-section view of phyllite at the location of sample 3779552. View towards the south, with moderate east-dipping deformation fabric. Note orange material is lichen. c. ~~Surface of shear fabric from locality of sample 3779551. d.~~ Cross section view of phyllite ~~in vicinity of sample 3779551. This field of view shows rafts of quartzite within the phyllite and complex buckling of the phyllitic-foliation, in places with a new shear fabric developed associated with these structures.~~ e_d. Detail of laminated metasiltstone of sample 3779554, showing high angle slaty cleavage developed and dipping steeply to the south-east (field of view looking towards north). ~~f. Poorly laminate~~d_e. Volcaniclastic sediment of the Heatherdale Shale from locality of sample 3779555.

4 ^{40}Ar/^{39}Ar analytical methods

As micas in these samples are very fine grained, ~~a~~ whole rock ~~approach was taken to mineral separation. In all cases except 3779551a and b, the separates~~ samples were ~~wholerock, including inseparable aggregates~~analysed, with the exception of ~~micas. In 3779551a and b the~~sample 3779551, from which aggregates of white mica were more prominent and were ~~therefore~~able to be separated and analysed. ~~Regions of the~~Whole rock ~~samples that were the focus of the geochronology were cut from the rock, for example areas where specific fabrics or minerals were located. Only the most pristine~~ material was ~~used from these selected areas. The cut out material was then~~ crushed and sieved to a 420-250μm size fraction. Hand picking was done to select the most suitable material/grains, ~~these were washed~~before washing in de-ionised water ~~until they were clean.~~. Necessary weights were calculated, and the weighed sample grains were packed into aluminium foils ~~and~~. The samples were then subjected to neutron irradiation at UC Davies nuclear reactor, USA for 12 hours and 5 minutes along with flux monitors, K_2SO_4 and CaF_2 salts for calculation of J-factors, monitoring corrections factors including ^{40}Ar production from potassium. Biotite standard GA-1550 ~~(99.769 ± 0.108 Ma; Renne et al., 2010) was used as the flux monitor.~~was used as the flux monitor. Furnace step-heating diffusion experiments were undertaken at the ^{40}Ar/^{39}Ar Laboratory, Research School of Earth Sciences, Australian National University, Canberra. Complete analytical details are given in Appendix B.

Analyses were conducted using a furnace step-heating procedure through an ultrahigh-vacuum extraction line to a *Thermo Fisher* ARGUS-VI multi-collector mass spectrometer. Step-heating diffusion experiments on individual samples were carried out with a temperature-controlled furnace that allows precise control of temperature during step-heating analysis, with heating schedules between 450°C and 1450 °C. ~~GA-1550 standards,~~The furnace was cleaned 4 times at 1450°C for 15 minutes each time prior to each new sample being loaded ensuring no cross-contamination between samples. Then low temperature baking of each sample is done whereby the sample is heated to 420°C for 3 minutes with the gas being pumped away then heated for 12 hours at 400 °C with the gas being pumped away. This was undertaken before each analysis to remove weakly held contaminant gas from non-lattice sites. GA-1550 standards were analysed using a CO_2 laser and a linear best fit was then used for the calculation of the J-factor and J-factor uncertainty. Data were reduced using *Noble* 2020 software using ~~the~~relevant correction factors and J-factors (Appendix B). Stated precisions for ^{40}Ar/^{39}Ar ages include all uncertainties in the measurement

of isotope ratios and are quoted at the one sigma level and exclude errors in the age of the flux monitor GA-1550. Reported data have been corrected for system backgrounds, mass discrimination, fluence gradients and atmospheric contamination. ^{40}K abundances and decay constants used are recommended values (Renne et al., 2010).(Renne et al., 2011). Result tables for each step heating experiment are given in Reid and Forster (2021), with a summary of these ages and their interpretations presented in Table 2. Weighted mean ages from selected steps are calculated in the case of three or more steps forming a coherent grouping, based on Pearson's chi statistic to assess whether the scatter remains within the 95% confidence limit and calculated using the software *eArgon* (see Muston et al., 2021 for detailed description of statistical methods).

5 ^{40}Ar/^{39}Ar age spectra results

All samples yield complex age spectra with multiple age populations (Fig. 5). Samples 3779553, 3779551a and 3779551b have similar age spectra that all have ages between c.470 and c. 459 Ma, obtained from between 20% and 70% of ^{39}Ar released. Mean ages calculated from these successive steps produce ages of 461.2 ± 1.6 Ma, 469.9 ± 1.3 Ma, and 459.2 ± 1.1 Ma for samples 3779553, 3779551a and 3779551b respectively, each defined by 95% confidence and a Pearson's chi statistic within acceptable range for a single population (see age calculation statistics in Appendix C). In each of these samples, the age spectra then step upwards towards significantly older ages, with maxima of c. 545 Ma, c. 1172 Ma and c. 1002 Ma respectively.

Sample 3779552 yielded some of the youngest age data from the samples in this study, with ages steadily rising from as young as c. 240 Ma to an upper limit of c. 477 Ma (Fig. 5b). Finally, samples 3779554 and 3779555, from the lowest metamorphic grade portions of the orogen (chlorite zone), yield age spectra with limits of c. 508 Ma and 530.3 ± 1.4 Ma (defined by ~50% ^{39}Ar released) respectively. These age spectra then increase in age to upper limits of c. 705 Ma and c. 567 Ma respectively. Both samples 3779554 and 3779555 have poorly defined lower limits c. 430 Ma, defined by the first 4 to 17% of ^{39}Ar released respectively.
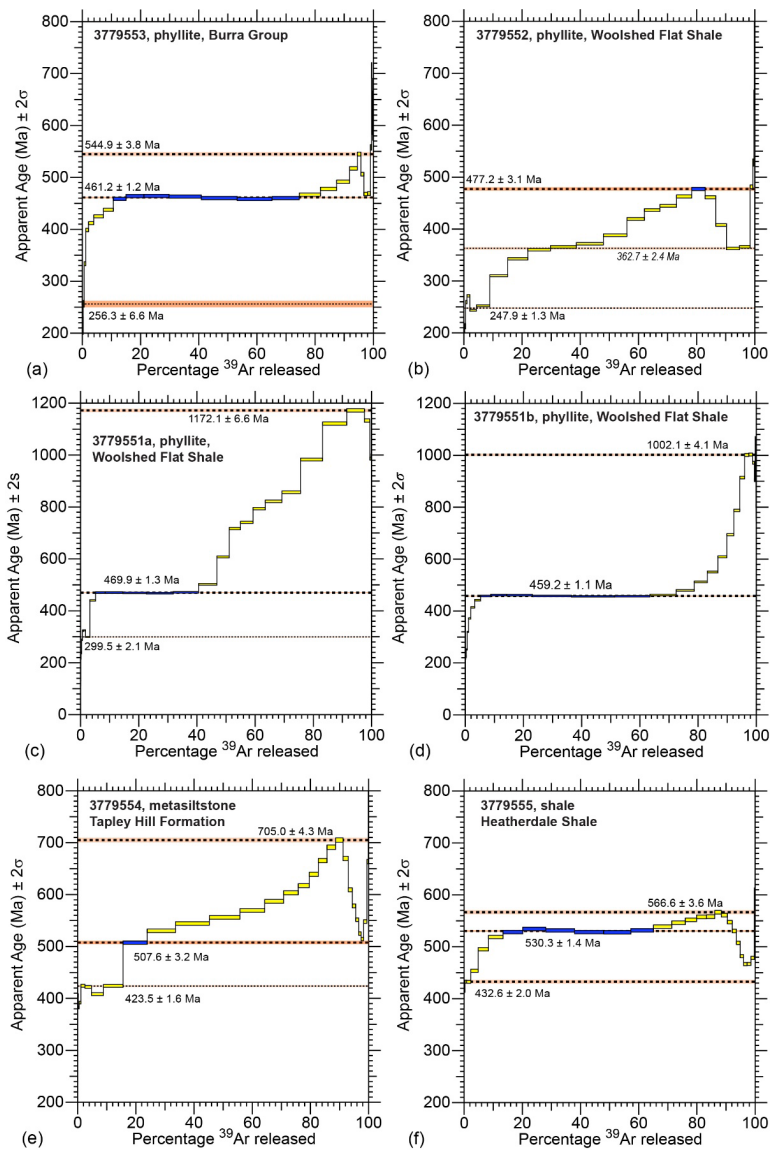
300

Figure 5: Apparent age spectra for samples analysed in this study. Age limits and asymptote (italicised in sample 3779552) defined using criteria of (Forster and Lister, 2004). All data tables are given in Reid and Forster (2021) a. Sample 3779553. b. Sample 3779552. c. Sample 3779551a. d. Sample ~~The age spectrum for sample 3779553 yields apparent ages that step progressively upwards over the first 18% gas released to a relatively flat portion of the spectrum to ~75% gas released (Fig. 5a). This flat portion yields an~~
305 ~~average age of 464.6 ± 4.5 Ma. The age spectra steps upwards from c. 464 Ma to a maximum of 549.5 ± 3.7 Ma, at step 21. The final portion of the age spectrum decreases in age to c. 464 Ma, before rising again to a maximum of 705 Ma. The York plot reveals the first 8 steps form a line of progressively decreasing ~~[36]~~Ar/~~[40]~~Ar ratio that represent a less retentive domain (Fig.~~ 3779551b. e. Sample 3779554. f. Sample 3779555.

~~5b). The final steps of the experiment yield progressively increasing [36]Ar/[40]Ar ratio, corresponding to higher retentive domain~~
310 ~~within the crystals.~~

~~Sample 3779552 has some of the youngest age data from the samples in this study. The first 10% of gas released has ages at 245.9 ±1.8 Ma (Fig. 5c). The ages rise from this minimum to an intermediate asymptote of 371.1 ± 7.8 Ma, while the upper age limit of 480.8 ±2.7 Ma occurs at around 80% gas release. The York plot shows that the early ages to have an atmospheric~~
315 ~~component, however, most of the heating steps have no or very minor atmospheric component with many steps represent mixing (Fig. 5d).~~

~~Two different separates of white mica were analysed from sample 3779551, denoted 3779551a and 3779551b. Sample 3779551a comprises silvery-coloured mica intergrown with shiny quartz grains, whereas the mica in sample 3779551b is~~
320 ~~greenish coloured. Sample 3779551a has an age of 473.1 ± 2.7 Ma that encompasses ~34% gas release, before stepping up to a much older maximum age of 1178.4 ± 5.4 Ma (Fig. 5e). [36]Ar/[40]Ar values have no atmospheric component, with exception of low volume steps at the initial and final portions of the step heating experiment (Fig. 5f). A similar pattern is found in sample 3779551b, which yields an age of 461.5 ± 3.9 Ma over ~54 % gas release, after which the spectrum steps upwards to a maximum age of 1007.8 ± 1.9 Ma (Fig. 5g). The York plot for sample 3779551b has two domains, with the majority with no~~
325 ~~atmospheric component and mixing in the beginning and final steps (Fig. 5h).~~

~~The age spectrum for sample 3779554 has apparent ages between c. 386 Ma and 426.9 Ma in the first 15% of [39]Ar release (Fig. 5i). At step 9 the age jumps to 511.3 ± 2.8 Ma and then rises consistently to a maximum of 709.6 ± 3.7 Ma at step 20. This staircase spectrum encompasses around 76% of gas released from the sample. After step 20, the age decreases to around~~
330 ~~c. <516 Ma. The York plot for sample 3779554 steps 1-8 define a population trending towards air composition, however, most steps have low to no to low atmospheric component (Fig. 5j).~~

~~Sample 3779555 yielded a lower age limit of 435.9 ± 0.4 Ma, rising to an intermediate age population of 532.9 ± 3.3 Ma (~45% [39]Ar released; Fig. 5k). The upper limit for this sample is an age of 564.2 ± 7.1 Ma. The York plot shows a small~~

335 ~~younger age cluster and the main cluster of steps with no atmospheric component, with mixing occurring between these to asymptotes/limits (Fig. 5l).~~
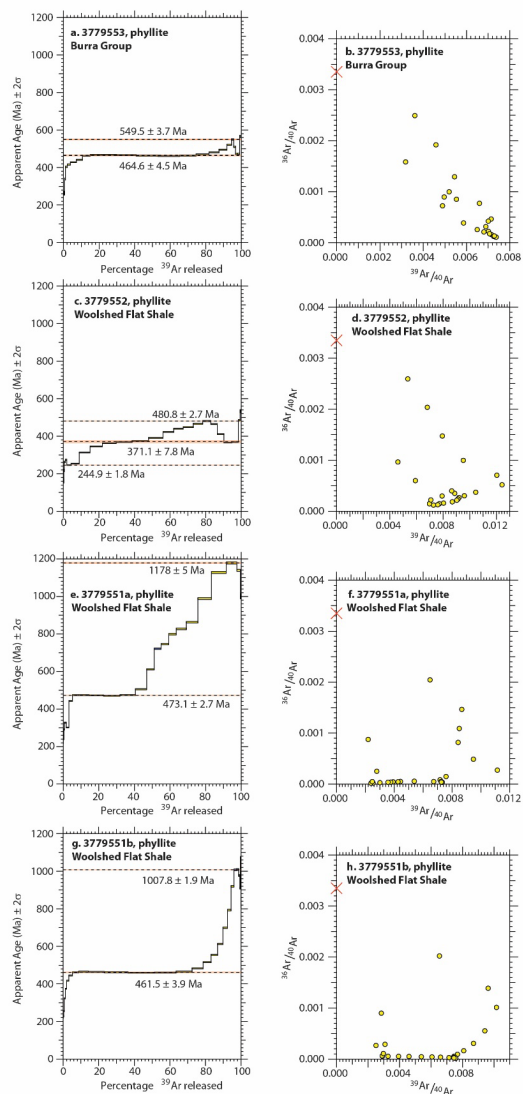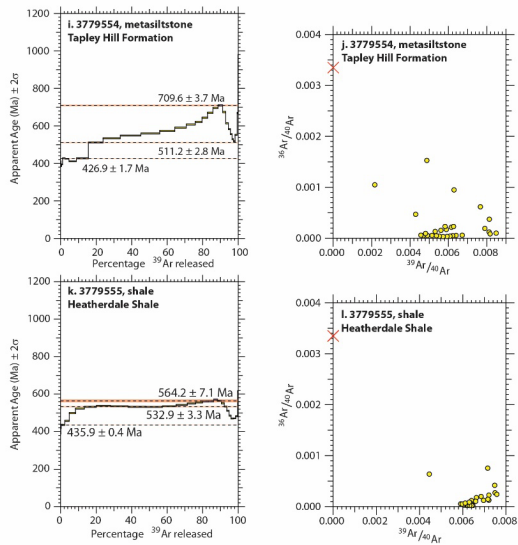
Figure 5: Apparent age spectra and corresponding York plots for samples analysed in this study. Note that all data tables are provided in Reid and Forster (2021) a. Sample 3779553 age spectrum. b. Sample 3779553 York plot. c. Sample 3779552 age spectrum. d. Sample 3779552 York plot. e. Sample 3779551a age spectrum. f. Sample 3779551a York plot. g. Sample 3779551b age spectrum. h. Sample 3779551b York plot. i. Sample 3779554 age spectrum. j. Sample 3779554 York plot. k. Sample 3779555 age spectrum. l. Sample 3779555 York plot.

Table 2. Summary of ^{40}Ar/^{39}Ar geochronology results.

Sample	Rock type	Stratigraphic unit	Minimum age Ma	Interpretation	Intermediate age Ma	Interpretation	Maximum age Ma	Interpretation
3779555	siltstone	Heatherdale Shale	435.9 ± 0.4	? Deformation	532.9 ± 3.3	Detrital	564.2 ± 7.1	Detrital
3779554	siltstone	Tapley Hill Formation	426.9 ± 2	? Deformation	511.3 ± 2.8	Metamorphism	709.6 ± 3.7	Detrital
3779551a	phyllite	Woolshed Flat Shale	473.1 ± 2.7	Deformation			1178.4 ± 5.4	Detrital
3779551b	phyllite	Woolshed Flat Shale	461.5 ± 3.9	Deformation			1007.8 ± 1.9	Detrital
3779552	phyllite	Woolshed Flat Shale	245.9 ±1.8	uncertain	371.1 ± 7.8	uncertain	480.8 ±2.7	Post-metamorphic cooling?
3779553	phyllite	Burra Group	465 ± 5	Deformation	549.5 ± 3.7	Partly reset detrital age		

6 Discussion

6.1 ~~Complex~~ Evaluation of ^{40}Ar/^{39}Ar ~~age spectra and York plots~~

350 ~~Single crystal or single mineral ^{40}Ar/^{39}Ar analysis on these samples is not possible due to the fine-grained nature of these~~ data quality from low- grade ~~tectono-~~metamorphic rocks. ~~As a consequence, complex ^{40}Ar/^{39}Ar age spectra are the mostly likely result. Complex ^{40}Ar/^{39}Ar age spectra can result from mixing of multiple age components within a whole rock sample caused by the mixing of different mineralogy~~

To interpret the complex ^{40}Ar/^{39}Ar age spectra obtained we firstly assess the reliability of the age data with respect to isotope
355 correlation diagrams, the relative abundance of radiogenic argon (^{40}Ar*) and the abundance of Ca- and Cl-derived ^{37}Ar and ^{38}Ar and cross-referencing this with mineralogical data derived from HyLogger^{TM}. Appendix C provides the complete set of relevant figures for each sample related to these isotopic data.

In each of the samples, isotope correlation diagrams between ^{36}Ar/^{40}Ar and ^{39}Ar/^{40}Ar show a similar pattern (Appendix C).
360 The first heating steps begin near the ^{36}Ar/^{40}Ar composition of air, track downwards towards very low values of ^{36}Ar/^{40}Ar. Most samples have ^{36}Ar/^{40}Ar values <0.002 for most heating steps. Significantly, the heating steps from which weighted mean ages are defined in 3779553, 3779551a, 3779551b and 3779555 all have low ^{36}Ar/^{40}Ar values that cluster. Typically, the final few steps in each sample trend towards higher ^{36}Ar/^{40}Ar values, possibly indicating release of ^{36}Ar in the final heating steps as mineral phases begin to break down under the high-temperature furnace conditions.
365

Mirroring the patterns in the isotope correlation diagrams, the lower temperature heating steps have correspondingly lower ^{40}Ar*, and often elevated Ca/K and Cl/K ratios (Appendix C). In some instances, this is correlated with younger ages, which may indicate recoil ^{39}Ar loss affects the first few percent of the age spectra. For this reason, the ages derived from the early heating steps must be considered with caution; it is unclear if the ages from early heating steps will have geological
370 significance. The elevated Ca and Cl values may further suggest argon from minerals such as plagioclase or chlorite may be influencing the ages from these lower temperature heating steps.

Sample 3779554 has higher Ca/K and Cl/K ratios (Appendix C) than any other sample. Interestingly, this sample has a relatively high proportion of albite compared to microcline and muscovite as recorded by thermal infrared spectroscopy
375 (Appendix A). The HyLogger^{TM} data also suggests relatively higher abundance of both calcite and dolomite in this sample, which may also be contributing to the elevated Ca/K ratios observed. The ^{40}Ar* values are relatively consistent, and the isotope correlation diagram suggests relatively low atmospheric component, implying that most of the age data are reliable and likely represents mixing between at least two 'virtual age components', one with an upper limit of c. 705 Ma and another with a lower limit of c. 507 Ma.
380

One potential issue with low grade metamorphic rocks is the presence of low temperature alteration (e.g. chlorite or clays) that can overprint the K-bearing phases such as muscovite, potentially leading to modification of the ages through recoil along fine grained mineralogical intergrowths (e.g. ~~Kula~~Lo and Onstott, 1989; Foland et al., ~~2010; Clauer, 2013~~1992; Di Vincenzo et al., 2003; Popov et al., 2019~~) or, in the case of single minerals or grains, as a result of different gas domains having a range of~~

385 ~~diffusion properties (e.g. Lovera et al., 1989; Muston et al., 2021). As discussed~~. Mineralogically, most samples are dominated by muscovite as the major K-bearing phase, although 3779554 and 3779555 have appreciable microcline in addition. Samples 3779551 and 3779553 contain chlorite, while sample 3779552 is dominated by chlorite (Appendix A). Ternary diagrams of ^{40}Ar*, K-derived ^{39}Ar and Cl-derived ^{37}Ar, reveal that ^{40}Ar* abundance dwarfs any contribution made by K- and Cl-derived argon, although we note the relatively large contribution of Ca-derived Ar to sample 3779552 (Fig. 6). This, together with the

390 discordance in the age spectrum, the variance in the isotope correlation diagram and the relatively large ^{37}Ar contribution suggest the results from this sample need to be treated with some caution. For the remaining samples however, we can be relatively confident that the age data from the high ^{40}Ar* heating steps is robust and can be interpreted to have geological significance.

395
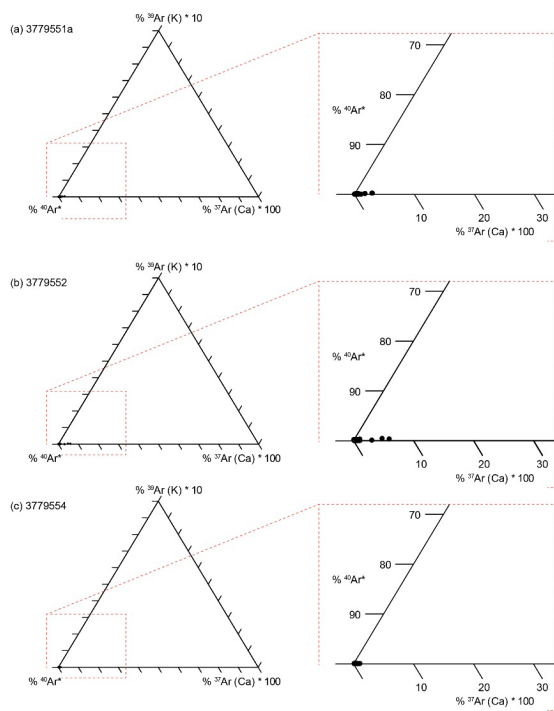
Figure 6. Representative ternary diagram for argon step heating data for three samples from this study, (a) 3779551a, (b) 3779552 and (c) 3779554. These ternary diagrams are based on those presented by Popov et al. (2019), and plot percentages of 40Ar*, K-derived ^{39}Ar and Cl-derived ^{37}Ar, where the ^{39}Ar(K) value is multiplied by 10, and the ^{37}Ar(Ca) value is multiplied by 100. These multiplication factors are required to make the individual heating steps visible on the ternary diagram; without these the variation in these two values is not visible, being two or more orders of magnitude smaller than ^{40}Ar* abundance.

6.2 Interpretation of complex ^{40}Ar/^{39}Ar age spectra from low grade metamorphic rocks

Now that we can say with some confidence that most of our age data is not significantly influenced by alteration, recoil, or other mineralogical effects, we turn to the problem of interpreting the complex age spectra themselves. In general, age spectra that have more than one plateau or plateau-like segment can be interpreted as containing a mixture of age populations, or virtual age components. Interpretation of such mixtures has been discussed in detail by Forster and Lister (2004), the ~~upper asymptote of a staircase age spectrum is the minimum age for crystallisation of the sample and conversely, the lower asymptote is a maximum age for either a less retentive domain within the sample, or a geological resetting event (Fig. 6a). Often complex~~

410 age spectra result from incomplete degassing of argon during one or more geological events, such as a thermal pulse or deformation event (Fig. 6b; e.g. Wijbrans and Mcdougall, 1988; Baldwin and Lister, 1998; Heizler et al., 1997). Similar staircase age profiles with upper and lower asymptotes have also been measured by whole rock analyses of phyllite from the Caledonian Orogen, Norway (Fig. 6c; Dallmeyer et al., 1988)key point being that mixtures can preserve, or partially preserve information on the timing of earlier episodes of cooling and/or deformation. Analysis of age spectra using asymptotes and

415 limits enables maximum and minimum constraints to be placed on the timing of the various events that the rock has been subjected to (Forster and Lister, 2004).

In multiply deformed tectonites, a record of earlier microstructures can be preserved especially in the cases where the temperatures and timescale at which cooling, deformation and recrystallisation occurred are not sufficiently strong so as to

420 completely outgas any older, relict mineral phases that may be present. Examples of this have been documented in analyses of white mica from the South Cyclades Shear Zone, Ios, where the complex age spectra reflect partial resetting during younger tectonic movement of the shear zone, in places with opposite kinematics (Fig. 7a; Forster and Lister, 2009). Similar staircase age profiles with upper and lower limits have also been measured by whole rock ^{40}Ar/^{39}Ar analyses of phyllite from the Caledonian Orogen, Norway (Fig. 7b; Dallmeyer et al., 1988). In the latter example, age gradients were interpreted to reflect

425 incomplete resetting of fine grained white mica during a Caledonian thermal event linked to emplacement of fold nappes onto the Baltic Shield (Dallmeyer et al., 1988). Numerous samples in our case study have very similar age profiles to those identified by Dallmeyer et al. (1988).

430
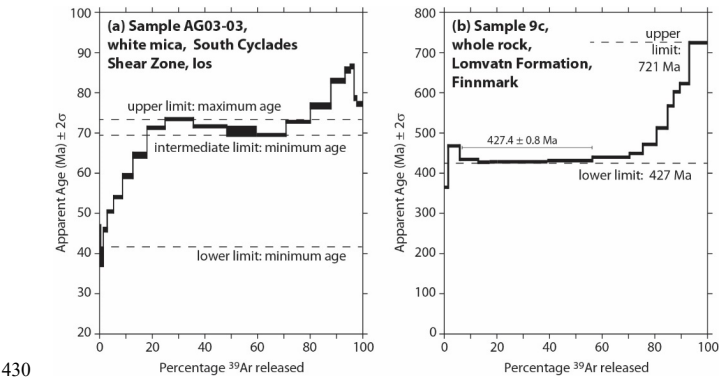
Figure 6. York plots, or inverse isochron plots, provide an insight into the isotopic composition of the argon released during step heating (Mcdougall and Harrison, 1999). An example of white mica from the South Cyclades Shear Zone, Ios, shows the

initial heating steps having a distinct isotopic composition, representing a mixing between atmospheric and the main mineral gas reservoir (Forster and Lister, 2009). This mixing is likely due to the effects of deformation-induced recrystallizationExample of complex age spectrum obtained from mixtures of minerals with different microstructural/microchemical compositions. (a) Sample of white mica from a South Cyclades Shear Zone, Ios, Greece, data from Forster and Lister (2009). The data are interpreted to contain three limits, and and lower limit. The upper and intermediate age limits are interpreted by (Forster and Lister, 2009). The main gas reservoir is also distinct from the high-temperature heating steps, which yield older apparent to reflect recrystallisation ages and represent mixing between atmospheric component and a minor excess ⁴⁰Ar component.

Complex age spectra and multiple gas domains are present in our samples from the low metamorphic grade rocks in the Delamerian Orogen. The presence of upper age asymptotesfabrics that also have distinct isotopic compositions, is consistent with those ages being from distinct gas reservoirs. Taken together, the complex age spectra in this study clearly represent the mixing between older detrital components and are relict from their earlier deformation, while the younger age components.
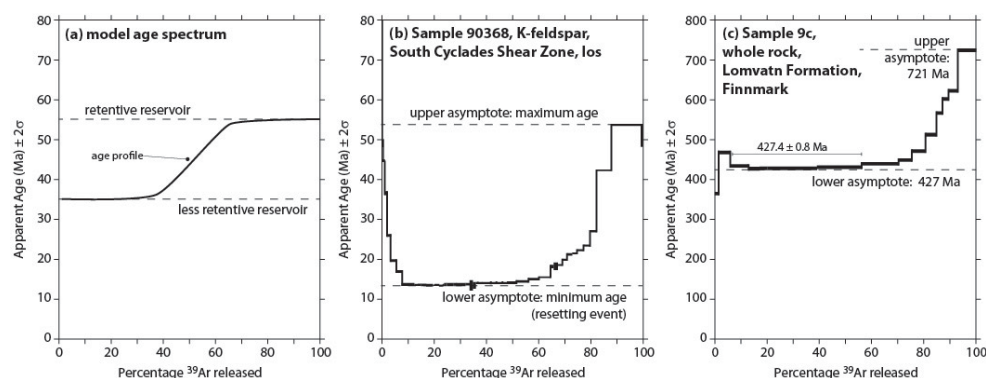
limit reflects partial modification of the Figure 6. Example complex age spectra. a. Model age spectrum of a simple age spectrum with two component system, mixing between more and less retentive argon gas reservoir. After Forster and Lister (2004). b. Example of K-feldspar with a staircase age spectrum patter resulting from degassing of two diffusion domains, with an upper asymptote defined by the more retentive domain providing a maximum age for the sample, and a lower asymptote representing the minimum age for resetting during greenschistHercynian amphibolite facies metamorphism. Age spectrum and interpretation after Baldwin and Lister (1998). (c. Example of complex age spectrum obtained from whole45 Ma). (b) Whole rock slate analysis from Dallmeyer

et al. (1988). The sample contains both detrital mica and a cleavage with the c. 427 Ma lower ~~asymptote~~limit interpreted to reflect timing of cleavage formation and the older ages the influence of detrital mineral with higher argon retentivity (Dallmeyer et al., 1988).

6.~~2~~3 Detrital ^{40}Ar/^{39}Ar signatures

Comparison of the different age spectra from our study reveals several features, which can be compared with the known depositional ages for the stratigraphic units as well as the timing of the Delamerian Orogeny established from higher grade regions of the orogen (Fig. 7). Firstly, the data reveal the presence of older ages that can be interpreted to be derived from detrital minerals preserved. The transport and deposition of K-bearing minerals can mean the ^{40}Ar/^{39}Ar signature of minerals within sedimentary rocks is representative of events in the source region, rather than indicative of new mineral growth or resetting. This principle has been applied in many settings to reconstruct the early history of orogenic regions now eroded (Stuart, 2002; Blewett et al., 2019), ~~including~~such as in the continental foreland basin of the Himalayas (Najman et al., 1997), and the Lachlan Orogen of eastern Australia (Fergusson and Phillips, 2001). ~~As discussed by Fergusson and Phillips (2001) the relative input of different detrital minerals in a whole rock analysis will depend on the abundance, grain size, argon retentivity and respective ages of the different detrital components.~~

~~In this study, the age spectra of most~~Two samples ~~contain ages~~ of the Woolshed Flat Shale of the Burra Group yield upper age limits of 1002 Ma and 1172 Ma (samples 3779551a and 3779551b), which are older than the ~~age of deposition of the rock. Therefore, these older components must be detrital in origin. Both aliquots~~c. 790 – 730 Ma depositional age range for this unit (Preiss, 2000; Lloyd et al., 2020). Hyperspectral analysis of sample ~~of the Woolshed Flat Shale (3779551) yielded the oldest apparently detrital ages, up to 1178 Ma and 1007 Ma.~~3779551 shows the dominant K-bearing mineral in the rock is muscovite. These Mesoproterozoic ages ~~are~~ potentially ~~reflecting~~reflect input of ~~material~~muscovite derived from the Musgrave Province or equivalent terranes of central Australia, as similar detrital ages are recorded in detrital zircon U-Pb studies of other rocks from the Adelaide Superbasin ~~(Lloyd et al., 2020). The oldest components are not the same age in each sample, and this may reflect the different character of the minerals in each. This variation may in turn relate to variation in composition of mica at the scale of individual laminations within the sample. The shape of the age spectra also suggests there is variation between these two sub-samples. In~~ (Ireland et al., 1998; Keeman et al., 2020; Lloyd et al., 2020). The ages are also consistent with the range of Mesoproterozoic ^{40}Ar/^{39}Ar ages obtained by single grain laser fusion methods by Haines et al. (2004) from other Neoproterozoic units in the region.

A third sample from the Burra Group, also dominated by muscovite in the hyperspectral data, yields a younger upper limit of 544 Ma (sample 3779553), considerably younger than the depositional age of the unit. In this sample ~~3779551b,~~ around 70%

of the ~~staircase portion of~~ ^{39}Ar release produces a pooled age of c. 461 Ma, with only the ~~age pattern begins at ~65 %~~ final ~17% of gas release ~~and is much steeper, compared to 3779551a. This suggests that 3779551b may have undergone a greater degree of recrystallisation at c. 460 Ma and consequently the c. 1007 Ma age represents a minimum detrital component.~~ ~~Increased~~ stepping upwards to older ages. This may suggest thermal and or microstructural overprinting ~~can have~~that has had the effect of drawing down the age of pre-existing age components in a sample. ~~The difference in these two age spectra suggests that even small degrees of recrystallisation, such as may occur in small~~ Indeed, the difference in both the shape of the age spectra and the upper age limit between the two Woolshed Flat Shale samples, 3779551a and 3779551b, also suggests that thermal and or microstructural overprinting has had a variable effect on these aliquots. The difference in these age spectra suggests that variation in the degrees of rate of cooling and or degree of recrystallisation in high strain zones ~~at the scale of a single hand sample,~~ can affect the ^{40}Ar/^{39}Ar composition of fine-grained rocks~~.~~, a result that mirrors the variation in recrystallisation documented in the shear zones of Ios by Forster and Lister (2009).

The remaining samples in this study yield apparent ages closer to their depositional age. Sample 3779554 yields an upper ~~asymptote~~limit of 709 Ma. ~~This~~The maximum depositional age of the Tapley Hill Formation, ~~quoted as~~ is 654 ± 13 Ma (U-Pb zircon; Lloyd et al., 2020)~~,~~ being very similar to the Re-Os date of 643.0 ± 2.4 Ma for the shale (Kendall et al., 2006), suggesting the age of the detrital minerals recorded by the ^{40}Ar/^{39}Ar data is ~~a minimum of ~50~~at least ~55 million years older than the depositional age. This sample is a laminated metasiltstone with a spaced cleavage~~.~~ and contains both microcline and muscovite in similar proportions. The ~~c. 511 Ma age likely approximates the timing of cleavage~~complexity in the age spectrum therefore relates to both variation in the relative contribution of K-feldspar and muscovite, as well as the probable influence of the formation ~~in this rock during the Delamerian Orogeny. The~~ of the spaced cleavage, which may have induced variable recrystallisation. The upper limit in the ^{40}Ar/^{39}Ar data is therefore a minimum estimate for the age of the detrital component.

The lowest metamorphic grade sample, ~~3779555~~ and the one with the least degree of strain is of the Heatherdale Shale~~,~~. This unit lies at the top of the Early Cambrian Normanville Group and contains tuffaceous zircons that crystallised at 514.98 ± 0.22 Ma (Betts et al., 2018), which constrains the timing of deposition. In our data, the Heatherdale Shale sample has upper ~~asymptote~~age limit of ~~564~~566.6 ± 3.6 Ma, ~~with~~and around 50% of ^{39}Ar released define a ~~younger limit of c. 532 Ma. This shale was deposited at c. 515 Ma (Betts et al., 2018), and consequently, the age spectra suggest that~~single age component of 530.3 ± 1.4 Ma. Both ages are older than deposition of the Heatherdale Shale and, given the rock is weakly deformed and underwent very low-grade metamorphism (chlorite facies from the regional metamorphic grade map, see Fig. 2), these ages must represent detrital mineral ages within the sample. The age spectrum suggests that very little of the K-bearing ~~minerals~~mineral in the shale ~~have~~has been reset either by diagenetic modification, or by younger tectonothermal processes ~~during the Delamerian Orogeny.~~. The minimal modification to the apparently detrital ^{40}Ar/^{39}Ar ages in this sample is consistent with the Heatherdale Shale being the stratigraphically youngest and least metamorphosed rock in this ~~sample set.~~

A further implication of these detrital mineral ages is to consider the concept that the difference in age between the youngest detritus and deposition of the rock is a response to tectonic setting. Cawood et al. (2012) show that detrital zircon ages in sediment from convergent plate margins are closer in age to the depositional age of the sediment compared to collisional, extensional and intracratonic basins, which contain greater proportions of older ages. On the basis of this relationship outlined by (Cawood et al., 2012) the presence of detrital Mesoproterozoic ^{40}Ar/^{39}Ar ages from the Neoproterozoic Woolshed Flat Shale implies that this deposited in an extensional basin, which is the inferred tectonic setting based on stratigraphic and tectonic reconstruction (Preiss, 2000). Conversely, the youngersample set.

In their single grain laser fusion ^{40}Ar/^{39}Ar study, Haines et al. (2004) show that the Carrackalinga Head Formation, which directly overlies the Heatherdale Shale, has detrital muscovite ages at c. 550–600 Ma and a minor peak at c. 950 Ma. The similarity to our data from the Heatherdale Shale supports the notion that very little resetting of the ^{40}Ar/^{39}Ar system has occurred in the detrital minerals of these units. We note, however, that assigning geological significance to the specific ages in our data set is difficult as both muscovite and microcline is present in the sample according to HyLogger^{TM} data. Consequently, it is not certain if the ages record cooling of, for example muscovite in the source region at c. 566 Ma and microcline at c. 530 Ma, or vice versa, or indeed if both virtual age components are mixtures of gas from both minerals. Further work on this sample could include attempts at mineral separation at fine scale to resolve detrital ^{40}Ar/^{39}Ar ages from the Heatherdale Shale.
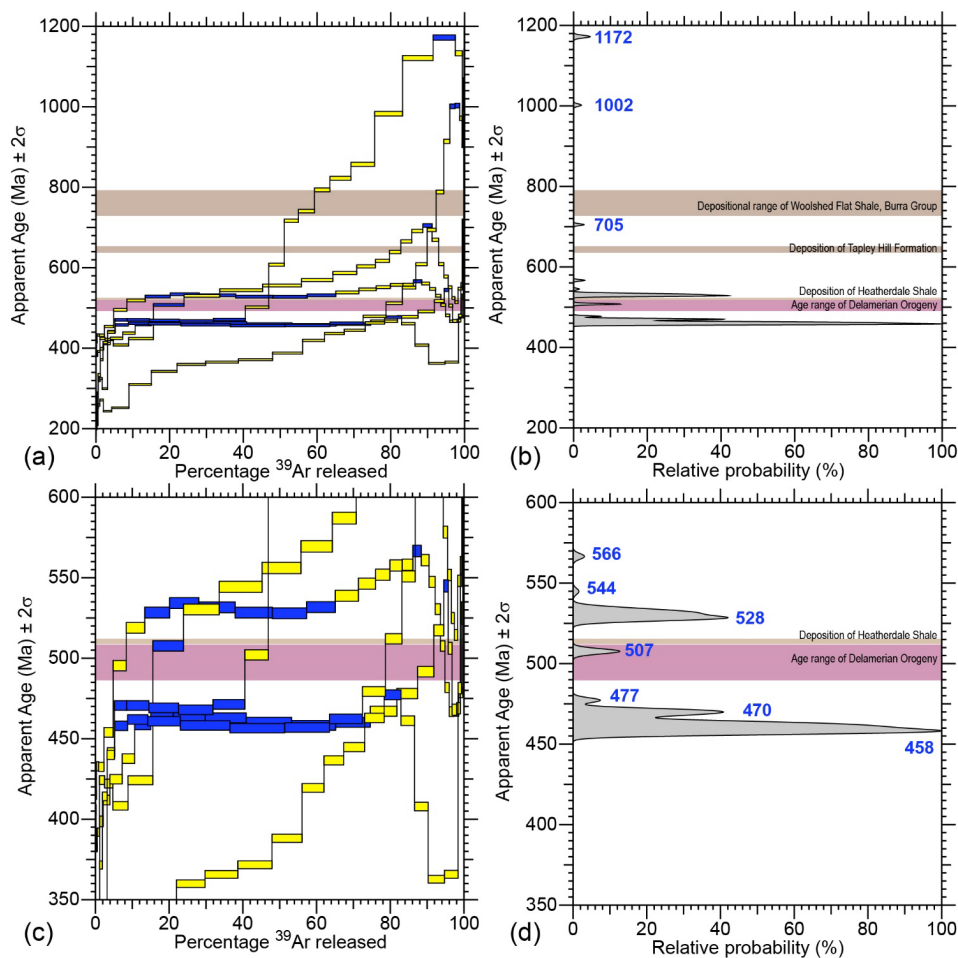
Figure 7. Synoptic plots that combine all age spectra and pooled Gaussian probability plots for the limits identified in each spectrum from this study. Steps highlighted blue have been either combined into pooled ages or as age limits. Gaussian plots calculated using the program eArgon and the methods described in detail by Muston et al. (2021) (a) Synoptic plot from 200 Ma to 1200 Ma. (b) Gaussian probability plot from 200 Ma to 1200 Ma. (c) Detailed synoptic plot from 350 Ma to 600 Ma. (d) Detailed gaussian probability plot from 350 Ma to 600 Ma.

6.4 Evidence for the c. 514 – 490 Ma Delamerian Orogeny in low grade rocks from the Delamerian Orogen

, c. 530 Ma component in the Heatherdale Shale, is within ~15 million years of the depositional age of this rock. This age relationship suggests the Cambrian sediments within the Delamerian Orogen formed in a basin setting related to a convergent margin. Indeed, although crustal extension followed immediately after deposition of the Heatherdale Shale with the formation of the Kanmantoo Trough this likely occurred in a back-arc setting, inboard of a newly initiated subduction system along the eastern margin of Gondwana (Foden et al., 2020).

The northern site (sample 3779553) and the Torrens Gorge locality (samples 3779551a and 3779551b) yielded significant portions of the age spectra at c. 460 Ma. In the Delamerian Orogen, syn-tectonic granites were emplaced at c. 514 – 500 Ma and post-tectonic granites at c. 485 Ma (Foden et al., 2006). The c. 460 Ma ages therefore do not lie within the time span of the Delamerian Orogeny as it is understood from the highest metamorphic grade regions of the orogen. This may indicate that the deformation in the thrust sheets that these samples are from continued until, or was active at c. 460 Ma, some 20 million years after the cessation of deformation in the high-metamorphic grade regions of the orogen. Alternatively, it is possible that the fine-grained nature of the samples means that the K-bearing mica in the sample 490 - 470 Ma, which bracket the timing of deformation to between c. 514 – 490 Ma (Foden et al., 2006; Foden et al., 2020). Somewhat surprisingly, only sample 3779554 of the Tapley Hill Formation has an age limit within the c. 514 – 490 Ma time range (Fig. 7). This limit is defined by a single step at c. 507 Ma at the start of the staircase age spectrum for this sample, which then rises to older ages derived from detrital or partially reset detrital minerals as discussed above. Where we have sampled it, the Tapley Hill Formation contains a weak spaced cleavage and lies within the chlorite isograd (see Fig. 2) suggesting relatively shallow burial, and it is possible that the c. 507 Ma age in this sample reflects the time at which this spaced cleavage formed. Nevertheless, in terms of frequently measured ages from this data set, evidence for recrystallisation or cooling during the c. 514 – 490 Ma Delamerian Orogeny is conspicuously absent.

The major ^{40}Ar/^{39}Ar age populations from this study instead lie between c. 470 Ma and c. 458 Ma (see Fig. 7d). These derive from muscovite-and chlorite-rich phyllite samples in the north of the study area, which are more deformed than either Tapley Hill Formation or Heatherdale Shale samples. These more deformed samples all have between 35% and 55% gas release defining the ages between c. 470 Ma and c. 458 Ma. We note that sample 3779552 yields an upper limit of c. 477 Ma age, defined by a single step and is of uncertain geological significance given the discordance of the age spectrum and the abundance of chlorite in this sample. We therefore focus the following discussion on the remaining samples and the ages between c. 470 Ma and c. 458 Ma, while recognizing that further sampling may reveal age populations that are older than c. 470 Ma and

therefore closer to the age of the Delamerian Orogeny recorded from higher grade zones within the orogen. The age data from
this study suggest that geological process or processes were operating in the western, low-grade region of the orogen some 20
to 32 million years after deformation in the high-grade region.

While our study has shown younger ages than the main time interval indicated for the Delamerian, we note that Turner et al.
(1994) and Turner et al. (2009) have also attempted to date low grade rocks from the orogen and instead produced ages older
than the typically quoted ages for Delamerian orogenesis. The single muscovite laser step-heating ^{40}Ar/^{39}Ar age spectrum
obtained by Turner et al. (2009) is very similar in form to the age spectra obtained in our study. Turner et al. (2009) averaged
a series of steps early in the heating experiment to yield an age of 533 ± 15 Ma, which they interpret as the timing of cleavage
formation. The higher temperature heating steps had significantly older ages (c. 850 – 900 Ma) they interpreted as detrital in
origin. If we reinterpret the muscovite sample of Turner et al. (2009) using the method of asymptotes and limits (Forster and
Lister, 2004), the age spectra has a lower limit of 499 ± 27 Ma (step 8 on their sample 01-HC-01). This could provide an
alternative estimate of the timing of cleavage formation, with the remainder of the spectrum being a result of mixing between
this younger limit and older detrital mineral ages. We note however, that Turner et al. (2009) present complimentary Rb/Sr
data on the same sample with an age of 554 ± 10 Ma, which they use to support the older age for the timing of cleavage
formation in these rocks. Turner et al. (2009) rule out mixing of older and younger populations in their analysis, however
considerable uncertainty remains about the significance of the Turner et al. (2009) and Turner et al. (1994) Rb/Sr isotopic data,
limited as it is to a single locality (see also discussion in Preiss, 1995b).

6.5 Cooling ages or deformation ages in fine grained samples

Regarding the c. 470 – 458 Ma frequently measured ages obtained in our ^{40}Ar/^{39}Ar data, we explore two interpretations as to
their significance:
1.   That these ages record passive cooling below the closure temperature or closure temperature range of the K-bearing
      minerals from an earlier deformation event that occurred above the closure temperatures of the component minerals.
2.   That these ages record the timing of recrystallisation of the minerals in the phyllite samples and therefore date the
      timing of deformation itself.

It is possible that the very fine-grained nature of the samples means that the K-bearing minerals in the samples may have
remained open to argon diffusion longer than might be expected if the samples were coarser-grained., since the rate of diffusion
is in part dependent on distance. As a result, thefine-grained samples may have continued to 'leak' argon until c. 460470 – 458
Ma when they finally were exhumed to shallow enough crustal levels.

to cool sufficiently to begin to retain radiogenic argon. In such a scenario, the shape of the age spectra itself can provide
information on the thermal evolution of a sample of a mixture of grains of different argon retentivity. Prolonged cooling

through a range of 'closure temperatures' in the detrital minerals and newly grown metamorphic micas may be expected to yield a staircase pattern in the age spectra, as a result of different argon ~~reservoirs cooling as~~'reservoirs' in the rock ~~passed~~cooling through a range ~~of closure temperatures, i.e. a closure temperature window. However, the age spectra for these~~

620 ~~samples have well-defined plateaus or plateau-like segments at c. 460 Ma, with relatively small portions of the age spectra actually having~~partial argon retention zones (Forster and Lister, 2004, 2010). In our study this type of staircase pattern is best exemplified by sample 3779554, in which over 85% of the age spectrum is a mixture between a minimum of c. 507 Ma and a maximum of c. 705 Ma. The weak cleavage in this sample supports the notion that most of the K-bearing mineral in the sample is detrital, with only a minor proportion being newly grown mica, possibly grown during formation of the spaced cleavage in

625 the Delamerian Orogeny.

If, on the other hand, more of the K-bearing minerals recrystallise during the deformation then one may expect to see a proportionally greater percentage of the age spectrum recording the younger age population. In such cases, the first portion of the age spectrum is likely to be a coherent age population (e.g. a plateau) derived from fine grained, less retentive newly grown

630 mica, which transitions via a staircase pattern. ~~In a~~ to older ages that are caused by the presence of incompletely reset/recrystallised detrital minerals. If small degrees of recrystallisation occurred, then we can reasonably expect to see only a small portion of the gas in the age spectrum to record the recrystallisation event. In our study, samples 3779553, 3779551a and 3779551b all show staircase-like age spectra with younger plateau segments stepping upwards to older ages. These samples are the most deformed of the samples we have analysed and have the highest proportion of muscovite in the mineralogical

635 data, with little evidence for microcline when compared to the samples from lower strain (3779554, 3779555). One possible interpretation is that the higher degree of strain in these samples resulted in breakdown of any possible detrital K-feldspar to form newly grown muscovite (and or biotite).

In general, phyllite forms at sub-greenschist to lower-greenschist facies temperatures (~ 200–300 °C) with the dominant

640 mineral assemblage being muscovite + chlorite + quartz (e.g. Palin and Dyck, 2021), which is the mineral assemblage of the phyllites sampled in this study. The ~ 200 – 300 °C temperature window is at the lower end of the spectrum of closure temperature windows expected for muscovite, which can be highly retentive depending on the composition (e.g. Harrison et al., 2009; Nteme et al., 2022). Therefore, we suggest that it is possible to interpret the plateau-like segments in our data from natural phyllites as recording the timing of muscovite recrystallisation and or growth in these rocks. We note also that in their

645 study of thrust sheets in the Norwegian Caledonides, ~~progressive changes in age spectra shape from samples~~Dallmeyer et al. (1988) show age spectra with very similar profiles resulting from deformation in the footwall of a thrust ~~in that study showed decreases in the degree of resetting, which Dallmeyer et al. (1988) interpreted to be a result of recrystallisation during~~, with the most deformed samples showing the increase in the percentage of the 'young' ages caused by thrusting~~.~~ (Fig. 6). The data presented here from the Delamerian Orogen has similar characteristics and ~~could~~can also be interpreted to indicate

650 recrystallisation of mica during ~~thrusting occurred~~deformation in the zones of phyllite at c. ~~460~~470 – 458 Ma. To further

investigate the possibility ~~of c. 460 Ma thrusting in the western Delamerian Orogen~~that the ages recorded in our study from the zones of phyllite are a result deformation, more samples could be taken progressively further away from the thrust zones to investigate ~~progressive changes in argon retentivity~~changes in argon age related to variation in factors such as deformation intensity, grain size and mineralogy of the shear zones.

655

If we interpret at least three of the age spectra presented here as recording the timing of deformation in the phyllitic thrusts at the western edge of the Delamerian Orogen, this implies that deformation in these thrust sheets was active at c. 470 – 458 Ma, which is at least 20 million years after the cessation of deformation in the high metamorphic grade regions of the orogen recorded in the ages of syn- to post-tectonic igneous intrusion (Foden et al., 2006). This interpretation produces several complications regarding how to account for the structural geology of the region. In the western Delamerian Orogen, cleavage foliations are axial planar to major regional folds with the intensity of cleavage development increasing and the orientation of the cleavage becoming shallower (east-dipping) especially on lower fold limbs, culminating in shear zones such as the ones sampled in this study (see fault-related folding in cross section of Figure 3 and also balanced cross sections of Flottmann and James, 1997; Flottmann et al., 1998). While it is possible that out of sequence thrusting could have occurred late in the deformation history after the main period of Delamerian deformation, the continuity of structure from low to high metamorphic grade regions across the orogen, raises the possibility that the c. 470 – 458 Ma ages record only the last phase of deformation in these thrust sheets, rather than the timing of inception of the thrusts themselves. We suggest a likely scenario is that these deformation zones are reactivated zones of weakness formed during earlier phases of the Delamerian Orogeny and possibly even earlier, as some of these structures formed during the Neoproterozoic and Cambrian rifting (Preiss, 1995a; Flottmann and James, 1997; Flottmann et al., 1998; Preiss, 2019). Therefore, although the c. 470 – 458 Ma ages are younger than the main ages for Delamerian deformation elsewhere in the orogen and were a surprising outcome of this study, there is no reason why these fault zones could not have been active, or continued to be active, during younger periods of deformation. Indeed, continued reactivation of older structures throughout the Phanerozoic is a feature of faults of the Mt Lofty Ranges, as detailed by Preiss (2019).

675

The c. 470 – 458 Ma activity recorded in our samples from thrusts of the western portion of the Delamerian Orogen is potentially related to far-field tectonic drivers along the then active eastern margin of Gondwana, now preserved in the adjacent Lachlan Orogen. Whilst tectonism associated with plate-margin processes to the east prior to c. 470 Ma had been primarily focused into the locally weak continental rift and back-arc basin, stabilisation of the Delamerian Orogen by c. 480 Ma may have facilitated far-field stresses being then transmitted across the whole orogen from the paleo-Pacific eastern margin of the Australian continent. The paleo-Pacific underwent several cycles of arc magmatism, accretionary tectonics, deformation and slab rollback during the Paleozoic (e.g. Glen, 2013; Rosenbaum, 2018, and others), and is a type example of an extensional accretionary orogen

In contrast, sample 3779552 has an upper age limit of 480 Ma and the age spectrum does show a stepwise progression of ages from ages as young as c. 245 Ma, with an intermediate age at c. 371 Ma. These ages are considerably younger than other ages obtained in this study and suggest that this sample has a complex history of mica growth and cooling. One interpretation of the spectrum could be that c. 480 Ma is a minimum age for peak metamorphism and deformation in the sample, recorded only in the higher temperature heating steps. Similar Early Ordovician ages are recorded in biotite from earlier K-Ar dating in the eastern Mt Lofty Ranges (Milnes et al., 1977; Turner et al., 1996). The even younger ages may record partial resetting of low retentivity domains within K-bearing minerals in the sample during the Carboniferous and Permian. Apatite fission track studies in the region also suggest exhumation at this time (Holford et al., 2021), possibly as a result of reactivation of faults across the southern Mt Lofty Ranges (Preiss, 2019). Sample 3779552 is from the hangingwall of the Para Fault, which has a neotectonic expression, and there is evidence that many of the neotectonic faults of the Adelaide region have been reactivated multiple times, sometimes involving reversal of movement sense (Preiss, 2019). Further dating in this region is required to better understand the context for the results obtained from sample 3779552.

In summary, the previous ^{40}Ar/^{39}Ar dating from the higher metamorphic grade regions and magmatic rocks of the Delamerian Orogen have suggested that cooling was relatively rapid, with exhumation of these rocks into the upper crust by c. 480 Ma (Turner et al., 1996). Importantly, these interpretations suggested that uplift of the Delamerian was rapid and connected to mantle upwelling, ie. lithospheric extension, as manifest also in the belt of post-tectonic and A-type granites in the region (TurnerCollins, 2002; Kemp et al., 1996; Foden et al., 20202009). Our new data on the rocks exposed in the western Mt Lofty Ranges suggest that this region was exhumed later than the higher metamorphic grade rocks in the east. This has implications for our understanding of the tectonic architecture of the Delamerian Orogen. It may suggest that some, if not all, of the major thrust sheets interpreted in the western Mt Lofty Ranges (Fig. 3) were active or, more likely, were re-activated at c. 460 Ma. Tectonic forces that led to these c. 460 Ma events are likely related to far-field drivers along the then active eastern margin of Gondwana, which is now preserved in the Lachlan Orogen (e.g. Moresi et al., 2014).

. Between c. 511 Ma to c. 500 Ma arc magmatism was concentrated in the Staveley Arc adjacent a west-dipping subduction system (Cayley and Skladzien, 2018; Lewis et al., 2018) and was broadly contemporaneous with the Delamerian Orogeny in the South Australian portion of the system. Intra-oceanic arc magmatism in the Macquarie Arc initiated outboard of this system as early as c. 503 Ma and continued to evolved through the Ordovician and into the Silurian (Kemp et al., 2020). Intriguingly, detailed stratigraphy and geochronology of the Macquarie Arc shows a series of 'phases' of magmatism and sedimentation, with the initial phase followed by a volcanic hiatus of c. 8 Myr, between c. 474 – 466 Ma (Glen et al., 2012). Although no precise correlation is necessarily implied, this hiatus in the Macquarie Arc partly corresponds to the timing of deformation inferred from the thrust zones in the Delamerian Orogen dated in this study. This may suggest there was some type of mechanical link between subduction dynamics along the paleo-Pacific margin and the activity along Delamerian thrust systems far inboard from the active margin.

7 Conclusion

Isotopic analyses of low-grade metamorphic ~~grade~~ rocks can be difficult to interpret as these are a mixture of detrital and newly grown, diagenetic or metamorphic minerals~~, which are not~~. As a consequence of this mixing, the isotopic signals from each of these components are not necessarily easy to resolve. In this study, we have applied the ^{40}Ar/^{39}Ar method with careful furnace step heating analysis of whole rock samples of low-grade metamorphic rocks. Key to interpreting the complex ^{40}Ar/^{39}Ar age spectra thus derived is the idea that the shape of the spectra themselves is informative as to the nature of the various gas reservoirs in a sample, and ~~asymptotes~~limits within the spectra define minimum and maximum ages for these components (Forster and Lister, 2004; Forster and Lister, 2009). In addition, examination of isotope correlation diagrams and ternary plots of ^{40}Ar*, ^{39}Ar(K) and ^{37}Ar(Ca) reveal the majority of gas in our samples is indeed radiogenic ^{40}Ar*, with the possible exception of one sample that has a significant proportion of chlorite. Data from this study shows that the Neoproterozoic rocks of the southern Delamerian Orogen preserve detrital mineral components up to ~~1178 Ma in age, while Cambrian shale yields detrital mineral components with ages of c. 564 and c. 532 Ma and hence much closer to the age of deposition. Applying the concept that younger detrital minerals are found in convergent margin sediment as has been shown from detrital zircon studies (Cawood et al., 2012), the new data from the Delamerian Orogen support the notion that the Cambrian was a time of convergent margin tectonics (i.e. subduction) along the eastern margin of Gondwana (Foden et al., 2020). Application of ^{40}Ar/^{39}Ar dating to low metamorphic grade successions across orogens with poorly defined tectonic settings may therefore be a useful tool to test tectonic settings, with implications for continental reconstruction models~~c. 1172 Ma in age, while Cambrian shale yields detrital mineral components with ages of c. 567 and c. 530 Ma, closer to the age of deposition.

~~Finally, the~~The younger ~~asymptotes~~limits in our data ~~are some~~occur in phyllitic samples with age segments at c. 470 – 458 Ma, which is at least 20 million years younger than the timing ~~of the last phases~~ of the Delamerian Orogeny documented from studies of granitic intrusions and amphibolite-grade metamorphic fabrics (Foden et al., 2006; Foden et al., 2020). ~~The two possible~~Two interpretations of the younger age components are (1) that they ~~are either (i) a~~record ~~of~~regional cooling, ~~with the minerals being passively cooled through their closure temperatures as a result of isotherm relaxation,~~ or ~~(ii) a~~2) record of deformation-induced recrystallisation~~.~~ at temperatures cooler than the closure temperature windows for the main K-bearing minerals in the phyllite. The second interpretation implies that some zones of phyllite in the Delamerian Orogen ~~could well have formed at, or continued until, sometime~~were active after the main phase of deformation recorded in higher metamorphic grade regions of the orogen. Potential coupling of stress transmitted from the distal plate margin along the paleo-Pacific margin of eastern Gondwana with the far-field continental interior may explain the (re)activation of some shear zones in the Delamerian Orogen. Further work is required to test these hypotheses, however, the new data point to the possibility that widespread application of this methodology, likely in combination with other methods such as Rb-Sr dating (e.g. Zack and Hogmalm, 2016), is a pathway forward for analysis of low-grade metamorphic ~~grade~~ rocks ~~as a complement~~. Certainly, the ^{40}Ar/^{39}Ar method is complementary to analysis of metamorphic rocks form higher grade regions within orogens by other

750 isotopic methods (e.g. zircon, monazite U-Pb) and ~~will provide a more~~provides for an holistic understanding of orogenic regions.

Appendix A. Hyperspectral mineralogical methods and results

Hyperspectral mineralogy methods

755 Samples were mineralogically characterised with a ~~Hylogger~~HyLogger-3™ (Schodlok et al., 2016), instrument at the Geological Survey of South Australia, Drill Core Reference Library, Adelaide. The HyLogger-3™ collects multiple data types including reflectance from the Visible-Near Infrared, Shortwave Infrared (VNIR-SWIR, 380-2,500 nm) and Thermal Infrared (TIR, 6,500 - 14,000 nm), high-resolution imagery and laser profilometer data at 4 mm resolution. Although this instrument is primarily designed to scan drill core, it is adaptable to collect data from a variety of geological materials. Each rock sample

760 was measured with five passes of the HyLogger™. The resulting spectral data was processed to exclude noisy and unwanted spectra using The Spectral Geologist™ v8.1.0.3 (TSG) software (Mason et al., 2020). Two algorithms, The Spectral Assistant™ (TSA) and joint Constrained Least Squares (jCLST), unmix the of spectral data and produces a semi-quantitative mineralogical result for SWIR and TIR. In this study, spectral results were obtained via traverses across each sample, with an average mineralogical composition compiled from both the SWIR and TIR spectrometers, as each wavelength range is

765 diagnostic for different minerals. Note that different minerals can appear in both SWIR and TIR analysis and that the total mineralogy identified by each spectral range is not necessarily indicative of the entire mineralogy of the sample. These data are used as a guide to the major mineral components, in particular the fine-grained minerals such as mica that are significant for the present $^{40}Ar/^{39}Ar$ study.

770 Scalars are algorithms applied within TSG designed to interpret diagnostic absorption features related to specific mineral species. A scalar developed by Haest et al. (2012) examines the wavelength change of the 2,200 nm Al-OH absorption feature (Figure A1), known to distinguish endmembers of white mica. Shorter wavelengths are indicative of a muscovitic composition and longer wavelengths demonstrate a phengitic white mica.

775 ~~Hylogger™~~HyLogger™ results for each sample are given in the following and are shown as:

    a) plain light high-resolution image of each sample,

    ~~b) the same image with the sample divided into a series of 'runs' in which the main mineralogy identified by SWIR and TIR analysis is shown in coloured bars below the image to demonstrate spatial variability within the sample, with the colour of the bars indicated in the adjacent legend,~~

780   ~~c)~~b) pie diagram compositional summary representing semi-quantitative HyLogger™ data identified in the SWIR wavelength range,

d)c) pie diagram compositional summary representing semi-quantitative HyLogger™ data identified in the TIR wavelength range.
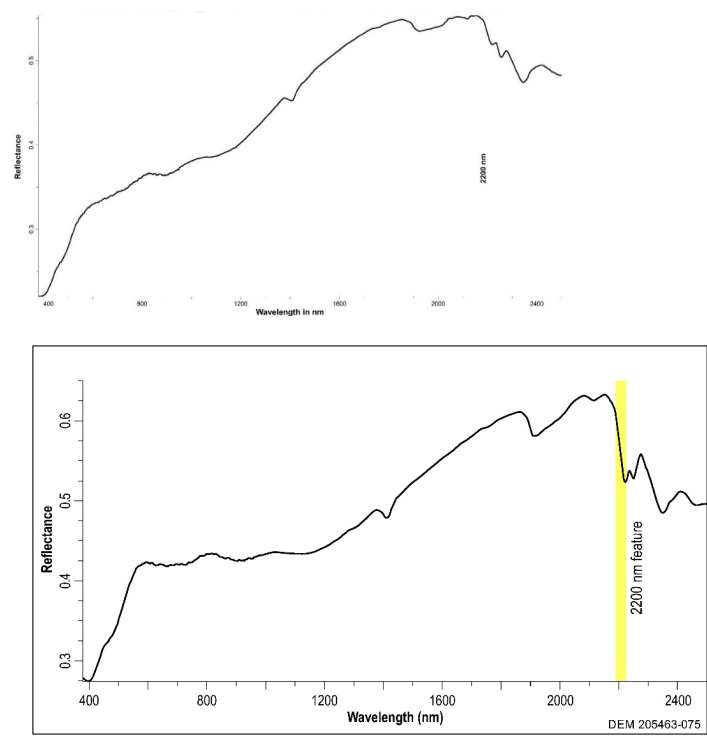
Figure A1. A representative spectral measurement from a sample in this study, the 2,200 nm feature is highlighted to demonstrate its position relative to the VNIR-SWIR spectral signature.

Hyperspectral mineralogy results for each sample analysed in this study
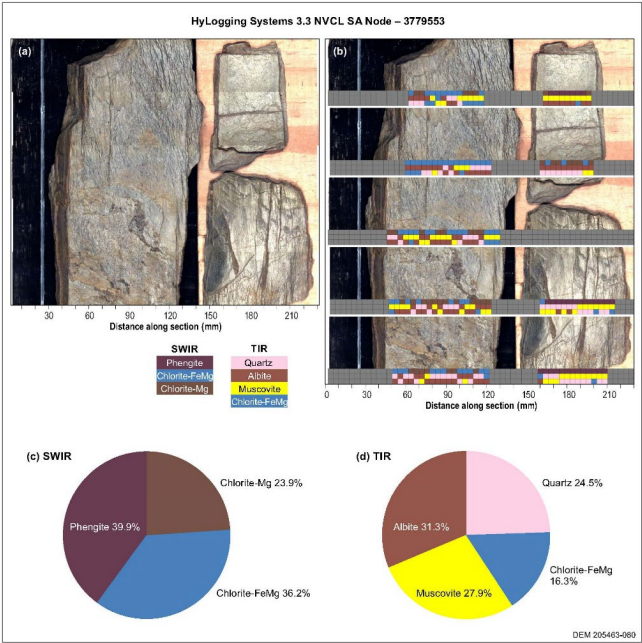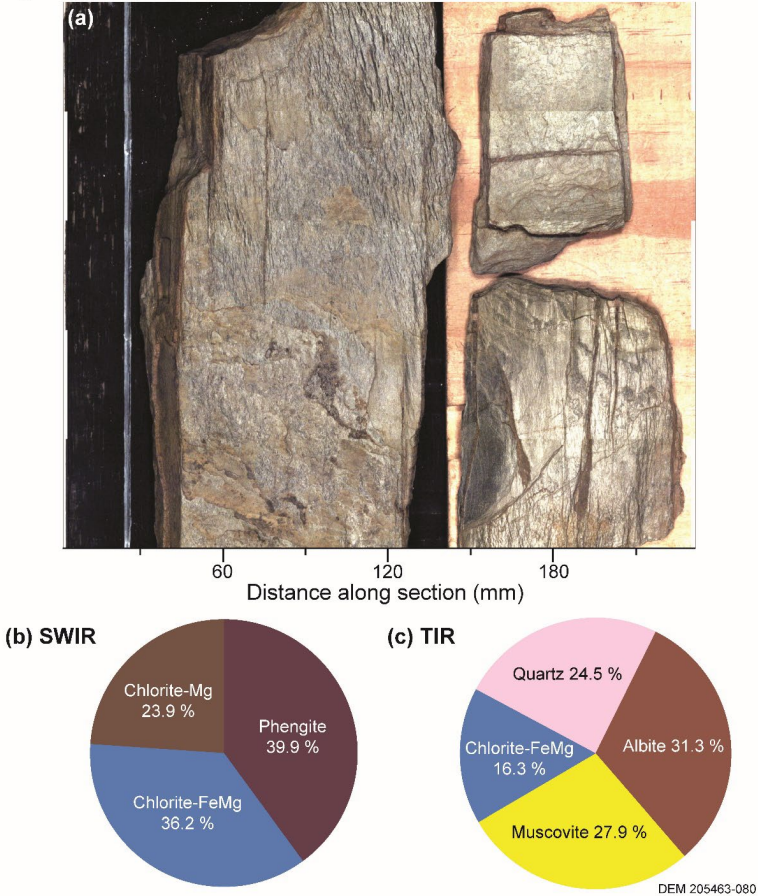
Figure A2. Hyperspectral mineralogy results for sample 3779553.
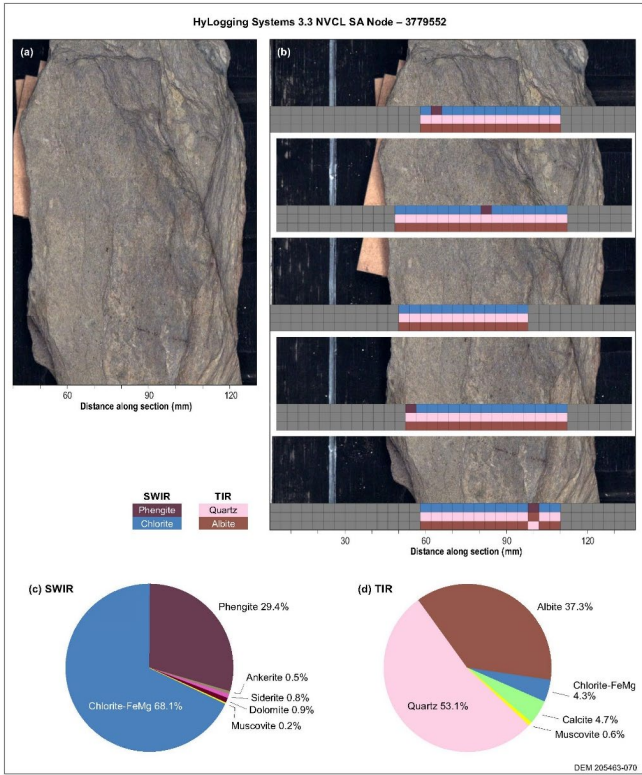
795
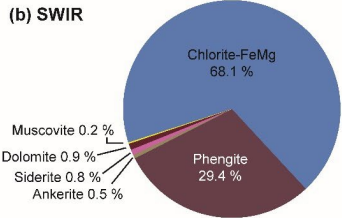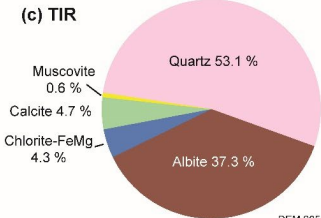
Figure A3. Hyperspectral mineralogy results for sample 3779552.
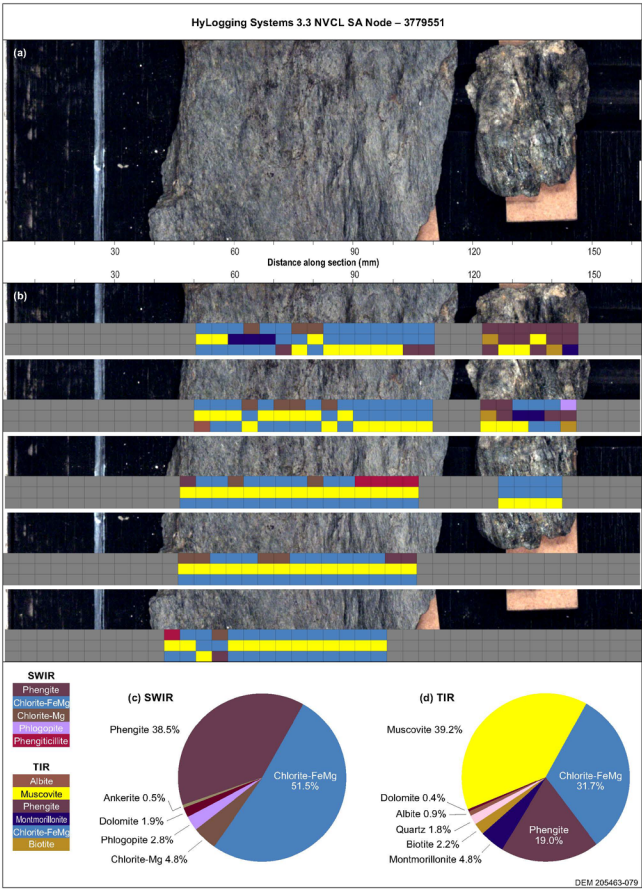
800
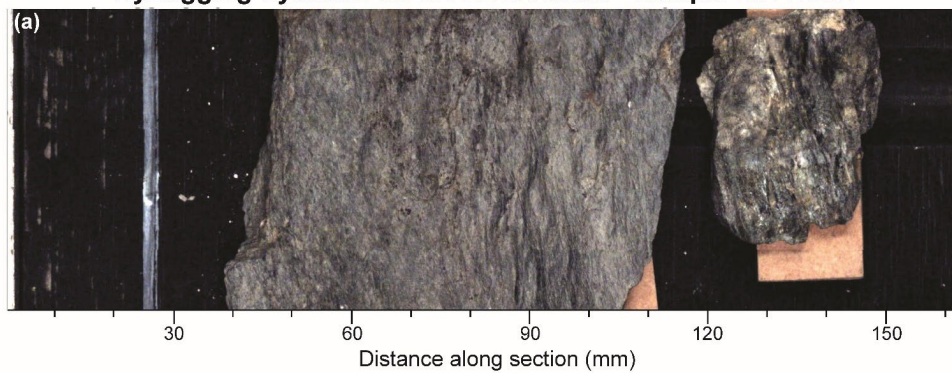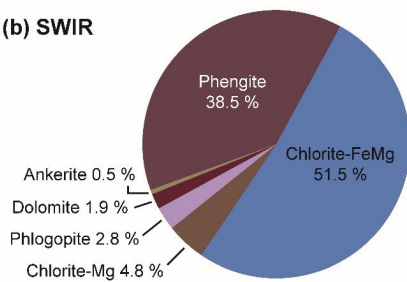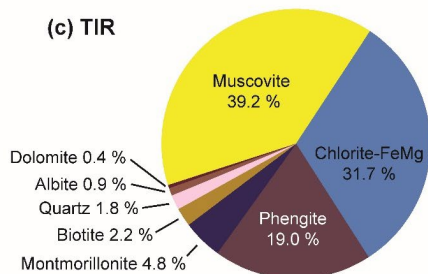
Figure A4. Hyperspectral mineralogy results for sample 3779551.

805
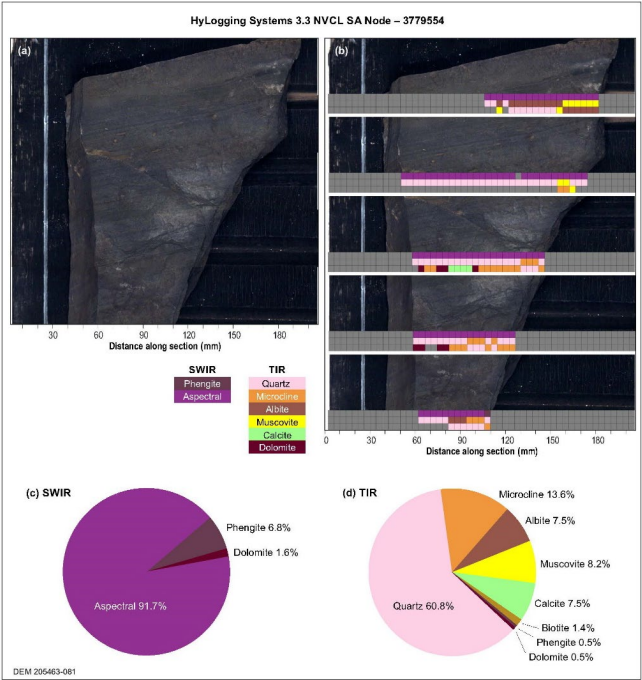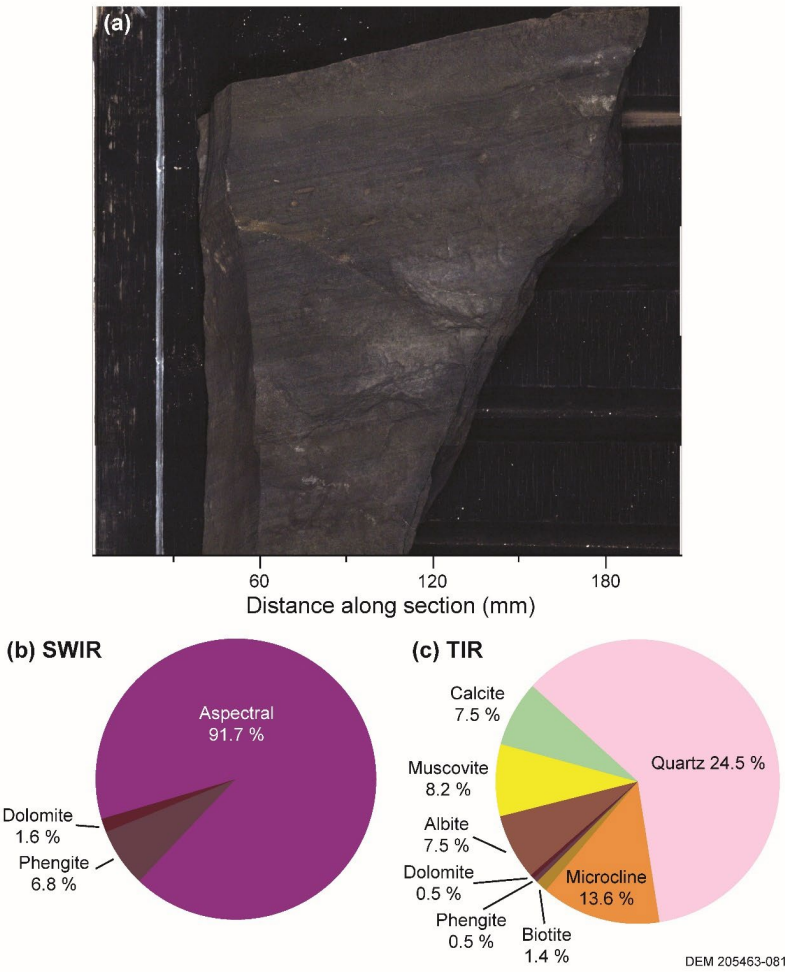
Figure A5. Hyperspectral mineralogy results for sample 3779554.
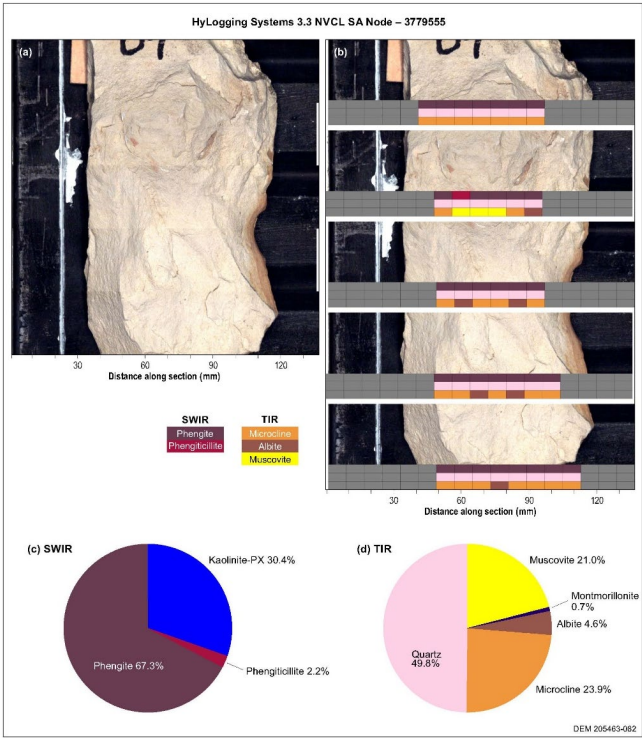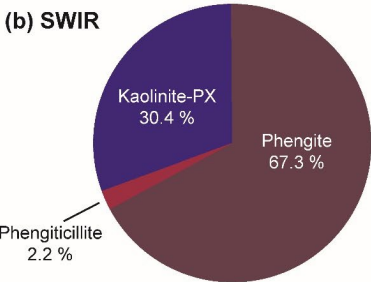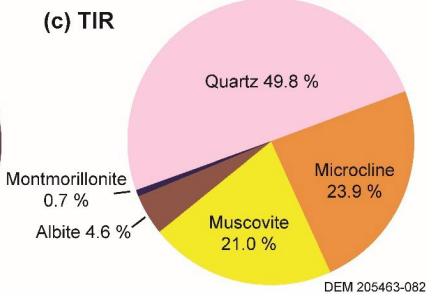
Figure A6. Hyperspectral mineralogy results for sample 3779555.

810

815 **References for Appendix A:**

Haest, M., Cudahy, T., Laukamp, C., and Gregory, S.: Quantitative Mineralogy from Infrared Spectroscopic Data. I. Validation of Mineral Abundance and Composition Scripts at the Rocklea Channel Iron Deposit in Western Australia, Economic Geology, 107, 209-228, 10.2113/econgeo.107.2.209, 2012.

Mason, P., Berman, M., Guo, Y., Warren, P., Lagerstrom, R., Bischof, L., Huntington, J., and Rodger, A.: The Spectral 820 Geologist (8.1.0.3), CSIRO [code], 2020.

Schodlok, M. C., Whitbourn, L., Huntington, J., Mason, P., Green, A., Berman, M., Coward, D., Connor, P., Wright, W., Jolivet, M., and Martinez, R.: HyLogger-3, a visible to shortwave and thermal infrared reflectance spectrometer system for drill core logging: functional description, Australian Journal of Earth Sciences, 63, 929-940, 10.1080/08120099.2016.1231133, 2016.

825

Appendix B. Details of ^{40}Ar/^{39}Ar analytical methods

Sample irradiation details:

Irradiation of samples for ^{40}Ar/^{39}Ar analysis is required, this was undertaken at the University of California Davis McClellan Nuclear Research Centre, CA, US. The samples in this study were wrapped in aluminium foil and irradiated in ANU CAN 830 #36 and the canister had 1.0mm cadmium shielding (Tetley et al., 1980). For each sample, calculated amounts of grains were weighed, recorded and wrapped in labelled aluminium packets in preparation for irradiation. The sample filled foils were placed into a quartz irradiation canister together with aliquots of the flux monitor GA1550. The GA1550 standards are dispersed throughout the irradiated canister, between the unknown age samples. In addition, packets containing K_2SO_4 and CaF_2 were placed in the middle of the canister to monitor ^{40}Ar production from potassium. Irradiated samples were unwrapped 835 upon their return to the Australian National University, and then rewrapped in tin foil in preparation for analysis in the mass spectrometer.

^{40}Ar/^{39}Ar procedures and analysis information:

Samples and standards were analysed in the Argon Laboratory at the Research School of Earth Science, The Australian 840 National University, Canberra, Australia using a *Thermo Fisher* ARGUS-VI multi-collector mass spectrometer. A furnace step-heating technique was used to extract argon isotopes from the samples to ensure 100% release of ^{39}Ar, while the flux monitors crystals (GA1550 biotite) were fused using a CO_2 continuous-wave laser; gases extracted from both the samples and standards were analysed in the Argus VI mass spectrometer. Samples had beenFor the furnace step-heating process, the samples were wrapped in tin foil so as to melt the tin and pump away the gases prior to the sample analysis. The furnace was 845 degassed 4 times at 1,450°C for 15 minutes and the gas pumped away prior to the loading of the subsequent sample. Gas

released from flux monitors and each step of sample analyses was exposed to three different Zr-Al getters to remove active gases for 10 minutes and the purified gas was isotopically analysed in the mass spectrometer. Samples were analysed with 30 steps and with temperatures of the overall schedule rising from 450° to 1,450°C (Reid and Forster, 2021). The $^{40}Ar/^{39}Ar$ dating technique is adapted from Mcdougall and Harrison (1999) and described in Forster and Lister (2009).

850

The background levels were measured and subtracted from all analysis, laser and furnace. For example, backgrounds were measured prior to every step of the sample analysis and subtracted from the isotope intensities for ^{40}Ar, ^{39}Ar, ^{38}Ar, ^{37}Ar and ^{36}Ar. The nuclear interfering values for the correction factors for the isotopes are listed below. These are measured for the reactions and uncertainties of $(^{36}Ar/^{37}Ar)_{Ca}$, $(^{39}Ar/^{37}Ar)_{Ca}$, $(^{40}Ar/^{39}Ar)_{K}$, $(^{38}Ar/^{39}Ar)_{K}$ and $(^{38}Ar)_{Cl}/(^{39}Ar)_{K}$, and were calculated

855   prior to sample analysis. The decay constant (Lambda^{40}K = 5.5305E-10) is based on the reported values in Renne et al. (2011).

Formatted: English (United Kingdom)

Formatted Table

ANU IRRADIATION CAN #36	
Flux Monitor: GA1550 @ 99.769 ±18 ± 0.108142 Ma (Renne et al 2010Intercalibration from Spell & McDougall 2003)	
$(^{36}Ar/^{37}Ar)_{Ca}$ correction factor	1.012835E-4
$(^{39}Ar/^{37}Ar)_{Ca}$ correction factor	8.469432E-4
$(^{40}Ar/^{39}Ar)_{K}$ correction factor	1.340092E-1
$^{38}Ar/^{39}Ar)_{K}$ correction factor	1.054454E-2
$(^{38}Ar)_{Cl}/(^{39}Ar)_{K}$ correction factor	8.184720E-2
Ca/K conversion factor	1.90
Discrimination factor	1.00441 ± 0.185%
Lambda ^{40}K	5.54920E5305E-10
Total irradiation power	12.08 MW
Irradiation Date	August 11-12, 2020

Sample	Field Way Point	Foil	J-Factor	J-Factor uncertainty	Mineral	Measurement Date
3779554	WP 12-01	M03	2.24374E-03	0.2425	Whole Rock	22 Mar,2021
3779555	WP 13-01	M11	2.23290E-03	0.2425	Whole Rock	24 Mar,2021
3779552	WPT 09-01	M17	2.22762E-03	0.2426	Whole Rock	30 Mar,2021
3779553	WPT 10	M21	2.22250E-03	0.2426	White Mica	12-Mar-2021
3779551a	WPT 5-01	M27	2.21396E-03	0.2427	Whole Rock	05 Apr,2021
3779551b	WPT 5-02	M28	2.21225E-03	0.2427	Whole Rock	06 Apr,2021

860 ^{40}K abundances and decay constants are calculated per ~~Renne et al. (2010).~~Renne et al. (2011). Stated precisions for ^{40}Ar/^{39}Ar ages include all uncertainties in the measurement of isotope ratios and are quoted at the one sigma level and exclude errors in the age of the fluence monitor GA1550 ~~(99.769 ±0.108 Ma);~~. The age of the flux monitor (GA1550 = 99.18 Ma) is based on the intercalibration value between GA1550 and Fish Canyon Sanidine age reported in Spell and Mcdougall (2003). The reported data have been corrected for system backgrounds, mass discrimination, fluence gradients and atmospheric 865 contamination. GA1550 standards were analysed and a linear best fit was then used for the calculation of the J-factor and J-factor uncertainty.

Data reductions were done with an adapted version of *Noble* Software (2020, written and adapted by the Australian National University Argon Laboratory). The data reduction was based on optimising MSWD (the mean square of weighted deviates) of 870 isotopes intensities with an exponential best fit methodology. The discrimination factor was calculated by analysing five Air Shots analysis on either side of sample analysis, based on the atmospheric ^{40}Ar/^{36}Ar ratio (298.57; see Lee et al., 2006), and the calculation of the 1amu was used for the discrimination factor.

^{40}Ar/^{39}Ar isotopic data of the sample is supplied in the Reid and Forster (2021), which includes details on: the heating schedule, 875 Argon isotopes abundances and uncertainty levels, %Ar*, ^{40}Ar*/^{39}Ar(K), Cumulative ^{39}Ar%, Age and uncertainty, Ca/K, Cl/K, J-factor and J-factor uncertainty, noting that the fractional uncertainties are shown as %, and are stated in the headings of the appropriate columns. Uncertainty levels of the calculated ages are at one sigma. Components involved in the calculation of the uncertainties are listed in the table below.

Uncertainty	Components involved in the calculation
Isotope Abundances	Uncertainty of isotope measurement Uncertainty of Mass Discrimination Factor (except for ^{39}Ar)
J-Factor	Uncertainty of ^{40}K Decay Constant Uncertainty of Age of the Flux monitor Uncertainty of Flux monitor isotopes abundances
Calculated Age	Uncertainty of Isotopes Abundances J-Factor value and uncertainty of J-Factor ^{40}K Decay Constant value and uncertainty of ^{40}K Decay Constant

880

Appendix C. Isotopic data plots for samples of this study.

For each sample, the age spectrum (a), isotope correlation diagram (b), percentage radiogenic ^{40}Ar (^{40}Ar*; c), Ca/K ratio (d) and Cl/K ratio (e) are presented. Below each set of plots is a description of the ages selected for combination or as single steps, along with statistical information on the pooled ages and the steps aggregated. Note that limits and asymptotes defined after Forster and Lister (2004); age plateau as per Schaen et al. (2020).

890
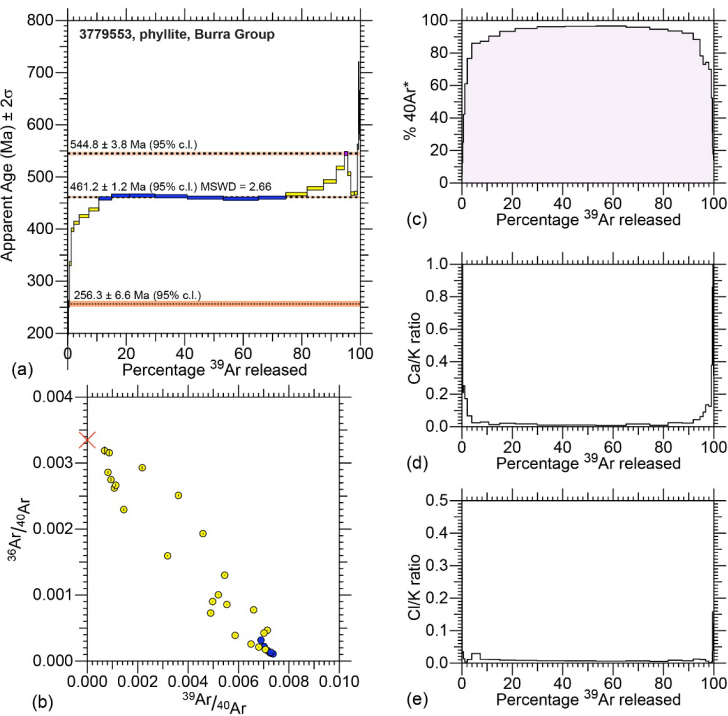
ANU CAN #36, Name: 3779553, Field ID: WPT 10, Foil: M21, Mineral: White Mica, Mass: 9.2mg, Steps: 30
Australia; SA; Burra Group; The Rocks; White-mica aggregates; clean fraction; Grain Size: 420-250micron

Plateau age 461.2 ± 1.16 Ma (95% c.l) Selected step(s): 10 11 12 13 14 15 16
Pearson's chi statistic 1.63 with 95% condence range f=6 [0.18 - 1.65].

Lower limit age 256.3 ± 6.55 Ma (95% c.l) Selected step(s): 4

Upper limit age 544.9 ± 3.79 Ma (95% c.l) Selected step(s): 21
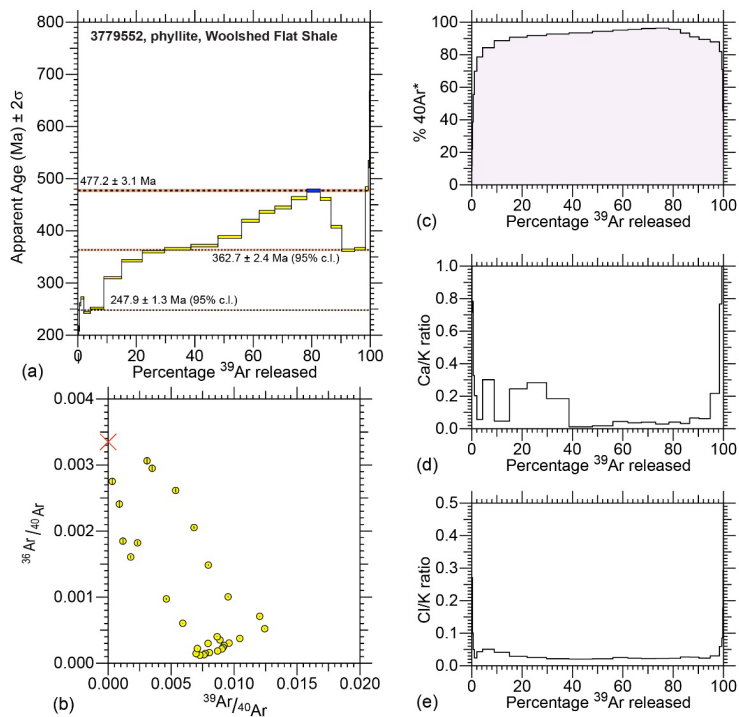
ANU CAN #36, Name: 3779552, Field ID: WPT 09-01, Foil: M17, Mineral: Whole Rock, Mass: 14.6mg, Steps: 30

Australia; SA; Woolshed Flat Shale; Deadmans Pass; Greenish white-mica aggregates with sheen; Grain Size: 420-250micron

Upper limit age 477.2 ± 3.05 Ma (95% c.l) Selected step(s): 19
Age based on selected steps 477.23 ± 3.05 Ma (95% c.l.)
Lower limit age 247.9 ± 1.25 Ma (95% c.l) Selected step(s): 7 8
Intermediate asymptote age 362.7 ± 2.41 Ma (95% c.l) Selected step(s): 22
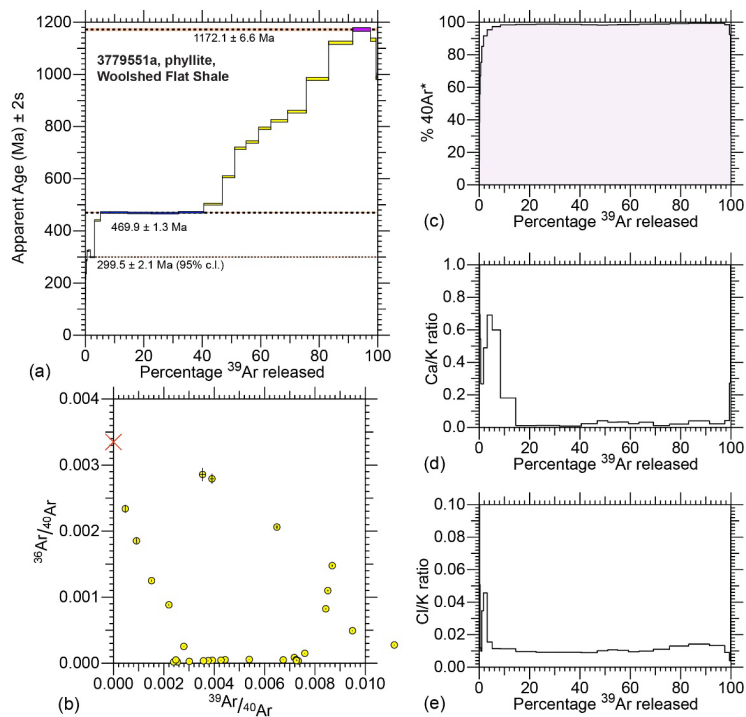
ANU CAN #36, Name: 3779551a, Field ID: WPT 5-01, Foil: M27, Mineral: Whole Rock, Mass: 10.3mg, Steps: 30

Australia; SA; Woolshed Flat Shale; Torrens Gorge; Mixture with greenish white-mica crystals and shiny quartz; Grain Size: 420-250micron

Uppper limit age 1172.1 ± 6.6 Ma (95% c.l) Selected step(s): 24

Pseudo-plateau age 469.9 ± 1.3 Ma (95% c.l) Selected step(s): 10 11 12 13 14
Pearson's chi statistic 0.92 with 95% confidence range f=4 [0.11 - 1.63]

Lowqer limit age 299.5 ± 2.1 Ma (95% c.l) Selected step(s): 8
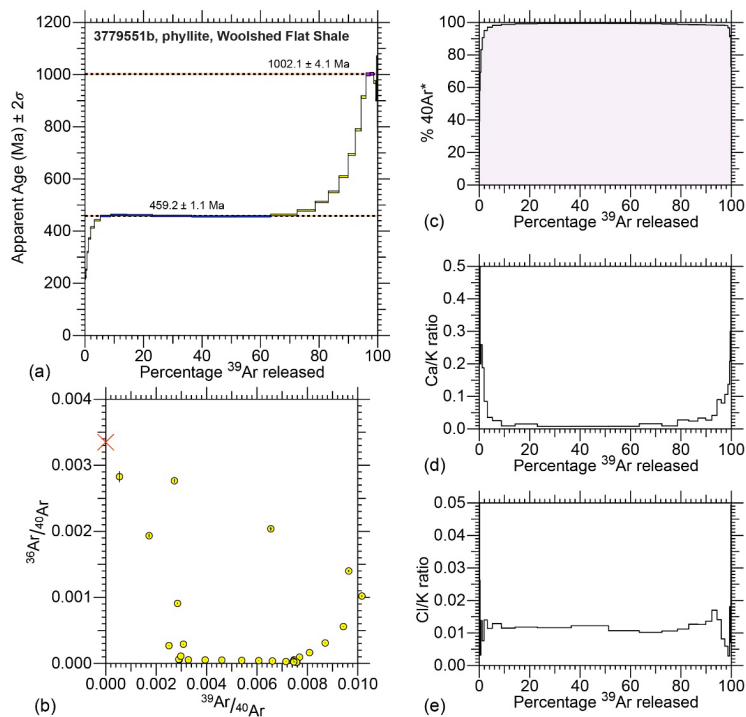
ANU CAN #36, Name: 3779551b, Field ID: WPT 5-02, Foil: M28, Mineral: Whole Rock, Mass: 10.3mg, Steps: 30

Australia; SA; Woolshed Flat Shale; Torrens Gorge; Greenish white-mica aggregates with sheen;
Grain Size: 420-250micron

Upper limit age 1002 ± 4.1 Ma (95% c.I) Selected step(s): 23 24

Plateau age 459.22 ± 1.11 Ma (95% c.I) Selected step(s): 9 10 11 12 13 14
Pearson's chi statistic 1.65 with 95% confidence range f=6 [0.18 - 1.65].
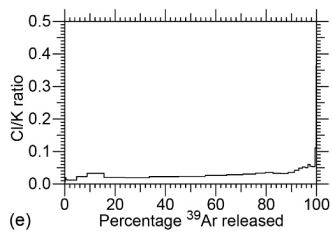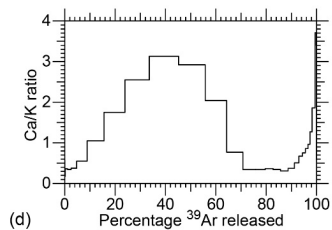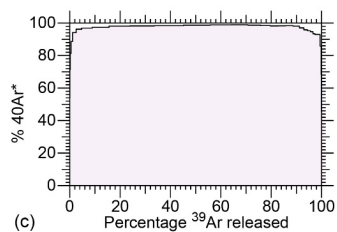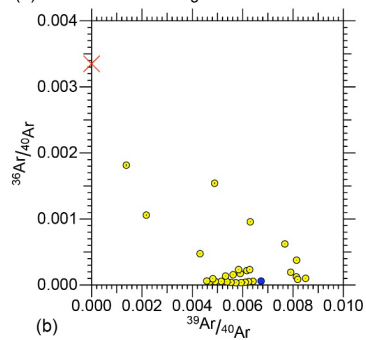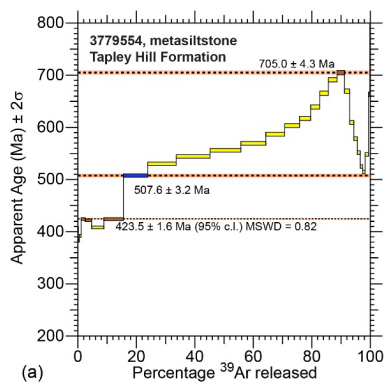
ANU CAN #36, Name: 3779554, Field ID: WP 12-01, Foil: M03, Mineral: Whole Rock, Mass: 70.3mg, Steps: 30

Australia; SA; Tapley Hill Formation; Tapley Hill; Slight shine whole-rock fraction; Grain Size: 420-250micron

Upper limit age 705.0 ± 4.33 Ma (95% c.l) Selected step(s): 20

Intermediate limit age 507.6 ± 3.23 Ma (95% c.l) Selected step(s): 9

Lower limit age 423.5 ± 1.59 Ma (95% c.l) Selected step(s): 5 6 8
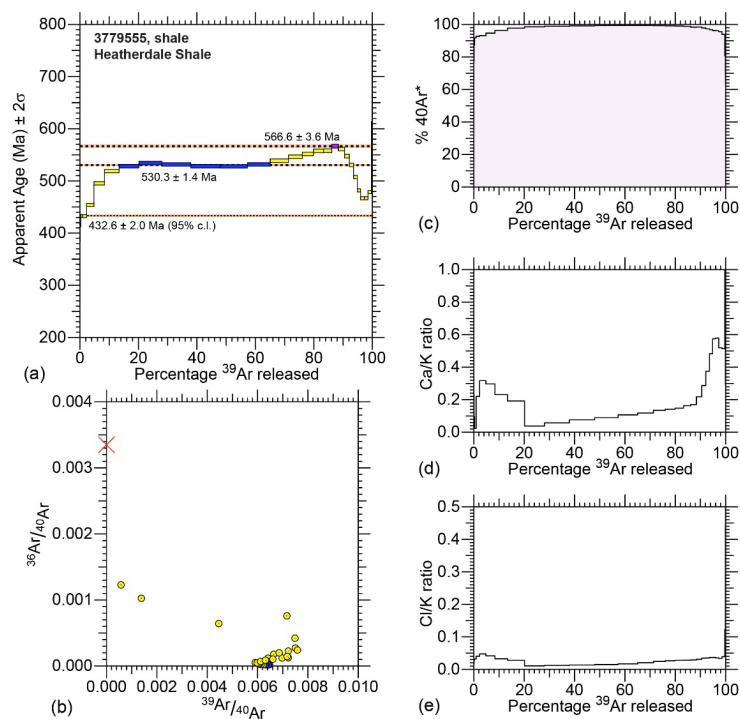
ANU CAN #36, Name: 3779555, Field ID: WP 13-01, Foil: M11, Mineral: Whole Rock, Mass: 100.4mg, Steps: 30

Australia; SA; Heatherdale Shale; Sellick Hill; Dark crystals with sheen; clean fraction; Grain Size: 420-250micron

Upper limit age 566.6 ± 3.57 Ma (95% c.I) Selected step(s): 19

Plateau age 530.3 ± 1.37 Ma (95% c.I) Selected step(s): 8 9 10 11 12 13
Pearson's chi statistic 1.52 with 95% confidence range f=5 [0.15 - 1.64].

Lower limit age 432.6 ± 2.00 Ma (95% c.I) Selected step(s): 3 4

Author contributions

Study design and field work by AR, MF, WP, SC. Sample preparation and analyses by MF, DV, GL, NG, AC. Interpretation and data analysis by all. AR prepared the manuscript with contributions from all co-authors.

Competing interests

The authors declare that they have no conflict of interest.

Acknowledgements

This work has been supported by the Mineral Exploration Cooperative Research Centre whose activities are funded by the Australian Government's Cooperative Research Centre Program. This is MinEx CRC Document 20**/***. The work is also supported by the Geological Survey of South Australia. Georgina Gordon is thanked for assistance with Hylogger™HyLogger™ analysis at the Department for Energy and Mining's South Australian Drill Core Reference Library, Adelaide. This study has benefited greatly from two insightful reviews by Jörg Pfänder and an anonymous reviewer.

References

Baldwin, S. L. and Lister, G. S.: Thermochronology of the South Cyclades Shear Zone, Ios, Greece: Effects of ductile shear in the argon partial retention zone, Journal of Geophysical Research: Solid Earth, 103, 7315-7336, https://doi.org/10.1029/97JB03106, 1998.

Betts, M. J., Paterson, J. R., Jacquet, S. M., Andrew, A. S., Hall, P. A., Jago, J. B., Jagodzinski, E. A., Preiss, W. V., Crowley, J. L., Brougham, T., Mathewson, C. P., García-Bellido, D. C., Topper, T. P., Skovsted, C. B., and Brock, G. A.: Early Cambrian chronostratigraphy and geochronology of South Australia, Earth-Science Reviews, 185, 498-543, https://doi.org/10.1016/j.earscirev.2018.06.005, 2018.

Blewett, S. C. J., Phillips, D., and Matchan, E. L.: Provenance of Cape Supergroup sediments and timing of Cape Fold Belt orogenesis: Constraints from high-precision 40Ar/39Ar dating of muscovite, Gondwana Research, 70, 201-221, https://doi.org/10.1016/j.gr.2019.01.009, 2019.

Burtt, A. C. and Phillips, D.: 40Ar/39Ar dating of muscovite from a pegmatite in Kinchina Quarry, near Murray Bridge, MESA Journal, 28, 50-52, 2003.

Cawood, P. A.: Terra Australis Orogen: Rodinia breakup and development of the Pacific and Iapetus margins of Gondwana during the Neoproterozoic and Paleozoic, Earth-Science Reviews, 69, 249-279, https://doi.org/10.1016/j.earscirev.2004.09.001, 2005.

Cawood, P. A., ~~Hawkesworth, C. J., and Dhuime, B.: Detrital zircon record and tectonic setting, Geology, 40, 875-878, 10.1130/g32945.1, 2012.~~

~~Cawood, P. A.,~~ Johnson, M. R. W., and Nemchin, A. A.: Early Palaeozoic orogenesis along the Indian margin of Gondwana:
930  Tectonic response to Gondwana assembly, Earth and Planetary Science Letters, 255, 70-84, https://doi.org/10.1016/j.epsl.2006.12.006, 2007.

Cayley, R. and Skladzien, P.: Structure, in: Regional geology and mineral systems of the Stavely Arc, western Victoria, edited by: Schofield, A., Record 2018/02. Geoscience Australia, Canberra. http://dx.doi.org/10.11636/Record.2018.002, 2018.

935 Chan, Y.-C., Crespi, J. M., and Hodges, K. V.: Dating cleavage formation in slates and phyllites with the 40Ar/39Ar laser microprobe: an example from the western New England Appalachians, USA, Terra Nova, 12, 264-271, https://doi.org/10.1046/j.1365-3121.2000.00308.x, 2000.

Clauer, N.: The K-Ar and 40Ar/39Ar methods revisited for dating fine-grained K-bearing clay minerals, Chemical Geology, 354, 163-185, 10.1016/j.chemgeo.2013.05.030, 2013.

940 Collins, W. J.: Nature of extensional accretionary orogens, Tectonics, 21, 1-6, 2002.

Cosca, M. A., Hunziker, J. C., Huon, S., and Masson, H.: Radiometric age constraints on mineral growth, metamorphism, and tectonism of the Gummfluh Klippe, Briançonnais domain of the Préalpes, Switzerland, Contributions to Mineralogy and Petrology, 112, 439-449, 10.1007/BF00310776, 1992.

Dallmeyer, R. D. and Takasu, A.: 40Ar/39Ar ages of detrital muscovite and whole-rock slate/phyllite, Narragansett Basin, RI-
945  MA, USA: implications for rejuvenation during very low-grade metamorphism, Contributions to Mineralogy and Petrology, 110, 515-527, 10.1007/BF00344085, 1992.

Dallmeyer, R. D., Mitchell, J. G., Pharaoh, T. C., Reuter, A., and Andresen, A.: K-Ar and 40Ar/39Ar whole-rock ages of slate/phyllite from allochthonous basement and cover in the tectonic windows of Finnmark, Norway: Evaluating the extent and timing of Caledonian tectonothermal activity, GSA Bulletin, 100, 1493-1501, 10.1130/0016-
950  7606(1988)100<1493:Kaaaaw>2.3.Co;2, 1988.

Di Vincenzo, G., Viti, C., and Rocchi, S.: The effect of chlorite interlayering on 40Ar–39Ar biotite dating: an 40Ar–39Ar laser-probe and TEM investigations of variably chloritised biotites, Contributions to Mineralogy and Petrology, 145, 643-658, 10.1007/s00410-003-0472-z, 2003.

Dunlap, W. J., Teyssier, C., McDougall, I., and Baldwin, S.: Ages of deformation from K/Ar and 40Ar/39Ar dating of white
955  micas, Geology, 19, 1213-1216, 10.1130/0091-7613(1991)019<1213:Aodfka>2.3.Co;2, 1991.

Dymoke, P. and Sandiford, M.: Phase relationships in Buchan facies series pelitic assemblages: calculations with application to andalusite-staurolite parageneses in the Mount Lofty Ranges, South Australia, Contributions to Mineralogy and Petrology, 110, 121-132, 10.1007/BF00310886, 1992.

Fergusson, C. L. and Phillips, D.: 40Ar/39Ar and K–Ar age constraints on the timing of regional deformation, south coast of
960  New South Wales, Lachlan Fold Belt: Problems and implications, Australian Journal of Earth Sciences, 48, 395-408, 10.1046/j.1440-0952.2001.00866.x, 2001.

Flottmann, T. and James, P.: Influence of basin architecture on the style of inversion and fold-thrust belt tectonics—the southern Adelaide Fold-Thrust Belt, South Australia, Journal of Structural Geology, 19, 1093-1110, https://doi.org/10.1016/S0191-8141(97)00033-3, 1997.

965 Flottmann, T., Haines, P., Jago, J., James, P., Belperio, A. P., and Gum, J.: Formation and reactivation of the Cambrian Kanmantoo Trough, SE Australia: implications for early Palaeozoic tectonics at eastern Gondwana's plate margin Journal of the Geological Society, 155, 525-539, 1998.

Foden, J., Elburg, M. A., Dougherty-Page, J., and Burtt, A.: The Timing and Duration of the Delamerian Orogeny: Correlation with the Ross Orogen and Implications for Gondwana Assembly, The Journal of Geology, 114, 189-210, 2006.

970 Foden, J., Sandiford, M., Dougherty-Page, J., and Williams, I.: Geochemistry and geochronology of the Rathjen Gneiss: Implications for the early tectonic evolution of the Delamerian Orogen, Australian Journal of Earth Sciences, 46, 377-389, 10.1046/j.1440-0952.1999.00712.x, 1999.

Foden, J., Elburg, M., Turner, S., Clark, C., Blades, M. L., Cox, G., Collins, A. S., Wolff, K., and George, C.: Cambro-Ordovician magmatism in the Delamerian orogeny: Implications for tectonic development of the southern
975  Gondwanan margin, Gondwana Research, 81, 490-521, https://doi.org/10.1016/j.gr.2019.12.006, 2020.

Foland, K. A., Hubacher, F. A., and Arehart, G. B.: 40Ar39Ar dating of very fine-grained samples: An encapsulated-vial procedure to overcome the problem of 39Ar recoil loss, Chemical Geology, 102, 269-276, https://doi.org/10.1016/0009-2541(92)90161-W, 1992.

Forster, M. and Lister, G.: Core-complex-related extension of the Aegean lithosphere initiated at the Eocene-Oligocene transition, Journal of Geophysical Research: Solid Earth, 114, https://doi.org/10.1029/2007JB005382, 2009.

Forster, M. A. and Lister, G. S.: The interpretation of 40Ar/39Ar apparent age spectra produced by mixing: application of the method of asymptotes and limits, Journal of Structural Geology, 26, 287-305, https://doi.org/10.1016/j.jsg.2003.10.004, 2004.

Forster, M. A. and Lister, G. S.: Argon enters the retentive zone: reassessment of diffusion parameters for K-feldspar in the South Cyclades Shear Zone, Ios, Greece, in: Advances in Interpretation of Geological Processes: Refinement of Multi-scale Data and Integration in Numerical Modelling, edited by: Spalla, M. I., Marotta, A. M., and Gosso, G., Geological Society of London, 10.1144/sp332.2, 2010.

Glen, R. A.: Refining accretionary orogen models for the Tasmanides of eastern Australia, Australian Journal of Earth Sciences, 60, 315-370, 10.1080/08120099.2013.772537, 2013.

Glen, R. A. and Cooper, R. A.: Evolution of the East Gondwana convergent margin in Antarctica, southern Australia and New Zealand from the Neoproterozoic to latest Devonian, Earth-Science Reviews, 220, 103687, https://doi.org/10.1016/j.earscirev.2021.103687, 2021.

Heizler, M. T., Ralser, S., and Karlstrom, K. E.: Late Proterozoic (Grenville?) deformation in central New Mexico determined from single-crystal muscovite 40Ar/39Ar age spectra, Precambrian Research, 84, 1-15, https://doi.org/10.1016/S0301-9268(96)00053-8, 1997.

Holford, S. P., Green, P. F., Duddy, I. R., Hillis, R. R., Hill, S. M., and Stoker, M. S.: Preservation of late Palaeozoic glacial rock surfaces by burial prior to Cenozoic exhumation, Fleurieu Peninsula, southeastern Australia, Journal of the Geological Society, 10.1144/jgs2020-250, 2021.

Glen, R. A., Quinn, C. D., and Cooke, D. R.: The Macquarie Arc, Lachlan Orogen, New South Wales: its evolution, tectonic setting and mineral deposits, Episodes, 35, 177-186, 10.18814/epiiugs/2012/v35i1/017, 2012.

Haines, P. W., Turner, S. P., Kelley, S. P., Wartho, J.-A., and Sherlock, S. C.: 40Ar–39Ar dating of detrital muscovite in provenance investigations: a case study from the Adelaide Rift Complex, South Australia, Earth and Planetary Science Letters, 227, 297-311, https://doi.org/10.1016/j.epsl.2004.08.020, 2004.

Harrison, T. M., Célérier, J., Aikman, A. B., Hermann, J., and Heizler, M. T.: Diffusion of 40Ar in muscovite, Geochimica et Cosmochimica Acta, 73, 1039-1051, https://doi.org/10.1016/j.gca.2008.09.038, 2009.

Ireland, T. R., Flottmann, T., Fanning, C. M., Gibson, G. M., and Preiss, W. V.: Development of the early Paleozoic Pacific margin of Gondwana from detrital-zircon ages across the Delamerian orogen, Geology, 26, 243-246, 1998.

Keeman, J., Turner, S., Haines, P. W., Belousova, E., Ireland, T., Brouwer, P., Foden, J., and Wörner, G.: New UPb, Hf and O isotope constraints on the provenance of sediments from the Adelaide Rift Complex – Documenting the key Neoproterozoic to early Cambrian succession, Gondwana Research, 83, 248-278, https://doi.org/10.1016/j.gr.2020.02.005, 2020.

Kemp, A. I. S., Blevin, P. L., and Norman, M. D.: A SIMS U-Pb (zircon) and Re-Os (molybdenite) isotope study of the early Paleozoic Macquarie Arc, southeastern Australia: Implications for the tectono-magmatic evolution of the paleo-Pacific margin, Gondwana Research, 82, 73-96, https://doi.org/10.1016/j.gr.2019.12.015, 2020.

Kemp, A. I. S., Hawkesworth, C. J., Collins, W. J., Gray, C. M., and Blevin, P. L.: Isotopic evidence for rapid continental growth in an extensional accretionary orogen: The Tasmanides, eastern Australia, Earth and Planetary Science Letters, 284, 455-466, http://dx.doi.org/10.1016/j.epsl.2009.05.011, 2009.

Kendall, B., Creaser, R. A., and Selby, D.: Re-Os geochronology of postglacial black shales in Australia: Constraints on the timing of "Sturtian" glaciation, Geology, 34, 729-732, 10.1130/g22775.1, 2006.

Kirkland, C. L., Daly, J. S., Chew, D. M., and Page, L. M.: The Finnmarkian Orogeny revisited: An isotopic investigation in eastern Finnmark, Arctic Norway, Tectonophysics, 460, 158-177, https://doi.org/10.1016/j.tecto.2008.08.001, 2008.

Kirschner, D. L., Masson, H., and Cosca, M. A.: An 40Ar/39Ar, Rb/Sr, and stable isotope study of micas in low-grade fold-and-thrust belt: an example from the Swiss Helvetic Alps, Contributions to Mineralogy and Petrology, 145, 460-480, 10.1007/s00410-003-0461-2, 2003.

Kula, J., Spell, T. L., and Zanetti, K. A.: 40Ar/39Ar analyses of artificially mixed micas and the treatment of complex age spectra from samples with multiple mica populations, Chemical Geology, 275, 67-77, https://doi.org/10.1016/j.chemgeo.2010.04.015, 2010.

Lee, J.-Y., Marti, K., Severinghaus, J. P., Kawamura, K., Yoo, H.-S., Lee, J. B., and Kim, J. S.: A redetermination of the isotopic abundances of atmospheric Ar, Geochimica et Cosmochimica Acta, 70, 4507-4512, https://doi.org/10.1016/j.gca.2006.06.1563, 2006.

Lewis, C., Huston, D., Schofield, A., Cayley, R. A., and Taylor, D.: New geochronology constraints on the development and duration of the Stavely Arc, in: Regional geology and mineral systems of the Stavely Arc, western Victoria, edited by: Schofield, A., Record 2018/02. Geoscience Australia, Canberra. http://dx.doi.org/10.11636/Record.2018.002, 2018.

Lloyd, J. C., Blades, M. L., Counts, J. W., Collins, A. S., Amos, K. J., Wade, B. P., Hall, J. W., Hore, S., Ball, A. L., Shahin, S., and Drabsch, M.: Neoproterozoic geochronology and provenance of the Adelaide Superbasin, Precambrian Research, 350, 105849, https://doi.org/10.1016/j.precamres.2020.105849, 2020.

Lovera, O. M., Richter, F. M., and Harrison, T. M.: The ^{40}Ar/^{39}Ar thermochonometry for slowly cooled samples having a distribution of diffusion domain sizes, Journal of Geophysical Research, 94, 17,917-917,935, 1989.

Lo, C.-H. and Onstott, T. C.: 39Ar recoil artifacts in chloritized biotite, Geochimica et Cosmochimica Acta, 53, 2697-2711, https://doi.org/10.1016/0016-7037(89)90141-5, 1989.

Mancktelow, N. S.: The structure of the southern Adelaide Fold Belt, South Australia, in: The evolution of a late Precambrian-early Paleozoic rift complex: the Adelaide Geosyncline, edited by: Jago, J. B., and Moore, P. S., Geological Society of Australia Special Publication 16, 369–395, 1990.

McDougall, I. and Harrison, T. M.: Geochronology and thermochronology by the ^{40}Ar/^{39}Ar method, 2nd, Oxford University Press, New York, 212 pp.1999.

Milnes, A. R., Compston, W., and Daily, B.: Pre- to syn-tectonic emplacement of early Palaeozoic granites in southeastern South Australia, Journal of the Geological Society of Australia, 24, 87-106, 10.1080/00167617708728969, 1977.

Moresi, L., Betts, P. G., Miller, M. S., and Cayley, R. A.: Dynamics of continental accretion, Nature, 508, 245-248, 10.1038/nature13033 http://www.nature.com/nature/journal/v508/n7495/abs/nature13033.html#supplementary-information, 2014.

Muston, J., Forster, M., Vasegh, D., Alderton, C., Crispin, S., and Lister, G.: Direct dating of overprinting fluid systems in the Martabe epithermal gold deposit using highly retentive alunite, Geochronology Discuss., 2021, 1-31, 10.5194/gchron-2021-25, 2021.

Najman, Y. M. R., Pringle, M. S., Johnson, M. R. W., Robertson, A. H. F., and Wijbrans, J. R.: Laser 40Ar/39Ar dating of single detrital muscovite grains from early foreland-basin sedimentary deposits in India: Implications for early Himalayan evolution, Geology, 25, 535-538, 10.1130/0091-7613(1997)025<0535:Laados>2.3.Co;2, 1997.

Nteme, J., Scaillet, S., Brault, P., and Tassan-Got, L.: Atomistic Simulations of 40Ar Diffusion in Muscovite, Geochimica et Cosmochimica Acta, https://doi.org/10.1016/j.gca.2022.05.004, 2022.

Offler, R. and Fleming, P. D.: A synthesis of folding and metamorphism in the Mt Lofty Ranges, South Australia, Journal of the Geological Society of Australia, 15, 245-266, 10.1080/00167616808728697, 1968.

Palin, R. M. and Dyck, B.: Metamorphism of Pelitic (Al-Rich) Rocks, in: Encyclopedia of Geology (Second Edition), edited by: Alderton, D., and Elias, S. A., Academic Press, Oxford, 445-456, https://doi.org/10.1016/B978-0-08-102908-4.00081-3, 2021.

Phillips, D., Fu, B., Wilson, C. J. L., Kendrick, M. A., Fairmaid, A. M., and Miller, J. M.: Timing of gold mineralisation in the western Lachlan Orogen, SE Australia: A critical overview, Australian Journal of Earth Sciences, 59, 495-525, 10.1080/08120099.2012.682738, 2012.

Popov, D. V., Brovchenko, V. D., Nekrylov, N. A., Plechov, P. Y., Spikings, R. A., Tyutyunnik, O. A., Krigman, L. V., Anosova, M. O., Kostitsyn, Y. A., and Soloviev, A. V.: Removing a mask of alteration: Geochemistry and age of the Karadag volcanic sequence in SE Crimea, Lithos, 324-325, 371-384, https://doi.org/10.1016/j.lithos.2018.11.024, 2019.

Preiss, W. V.: The Adelaide Geosyncline: Late Proterozoic stratigraphy, sedimentation, palaeontology and tectonics, Geological Survey of South Australia - Bulletin 53, Adelaide, 428 pp.1987.

Preiss, W. V.: Delamerian Orogeny, in: The geology of South Australia; Volume 2, The Phanerozoic, edited by: Drexel, J. F., Preiss, W. V., and Parker, A. J., Geological Survey of South Australia - Bulletin 54 Adelaide, 45-59, 19951995a.

Preiss, W. V.: RbSr dating of differentiated cleavage from the upper Adelaidean metasediments at Hallett Cove, southern Adelaide fold belt: Discussion, Journal of Structural Geology, 17, 1797-1800, https://doi.org/10.1016/0191-8141(95)00094-T, 1995b.

Preiss, W. V.: The Adelaide Geosyncline of South Australia and its significance in Neoproterozoic continental reconstruction, Precambrian Research, 100, 21-63, 2000.

Preiss, W. V.: The tectonic history of Adelaide's scarp-forming faults, Australian Journal of Earth Sciences, 66, 305-365, 10.1080/08120099.2018.1546228, 2019.

Reid, A. and Forster, M., 2021, Complex 40Ar/39Ar age spectra from low metamorphic grade rocks, Delamerian Orogen, Reid et al, Mendeley Data, V1, doi: 10.17632/g75hgmypbw.1

Renne, P. R., Mundil, R., Balco, G., Min, K., and Ludwig, K. R.: R., Mundil, R., and Min, K.: Response to the comment by W.H. Schwarz et al. on "Joint determination of 40K decay constants and 40Ar∗/40K for the Fish Canyon sanidine standard, and improved accuracy for 40Ar/39Ar geochronology." by P.R. Renne et al. (2010), Geochimica et Cosmochimica Acta, 74, 5349-5367, 10.1016/j.gca.2010.06.017, 201075, 5097-5100, https://doi.org/10.1016/j.gca.2011.06.021, 2011.

Rosenbaum, G.: The Tasmanides: Phanerozoic Tectonic Evolution of Eastern Australia, Annual Review of Earth and Planetary Sciences, 46, 291-325, 10.1146/annurev-earth-082517-010146, 2018.

Schaen, A. J., Jicha, B. R., Hodges, K. V., Vermeesch, P., Stelten, M. E., Mercer, C. M., Phillips, D., Rivera, T. A., Jourdan, F., Matchan, E. L., Hemming, S. R., Morgan, L. E., Kelley, S. P., Cassata, W. S., Heizler, M. T., Vasconcelos, P. M., Benowitz, J. A., Koppers, A. A. P., Mark, D. F., Niespolo, E. M., Sprain, C. J., Hames, W. E., Kuiper, K. F., Turrin, B. D., Renne, P. R., Ross, J., Nomade, S., Guillou, H., Webb, L. E., Cohen, B. A., Calvert, A. T., Joyce, N., Ganerod, M., Wijbrans, J., Ishizuka, O., He, H., Ramirez, A., Pfänder, J. A., Lopez-Martínez, M., Qiu, H., and Singer, B. S.: Interpreting and reporting 40Ar/39Ar geochronologic data, GSA Bulletin, 133, 461-487, 10.1130/b35560.1, 2020.

Schodlok, M. C., Whitbourn, L., Huntington, J., Mason, P., Green, A., Berman, M., Coward, D., Connor, P., Wright, W., Jolivet, M., and Martinez, R.: HyLogger-3, a visible to shortwave and thermal infrared reflectance spectrometer system for drill core logging: functional description, Australian Journal of Earth Sciences, 63, 929-940, 10.1080/08120099.2016.1231133, 2016.

Spell, T. L. and McDougall, I.: Characterization and calibration of 40Ar/39Ar dating standards, Chemical Geology, 198, 189-211, https://doi.org/10.1016/S0009-2541(03)00005-6, 2003.

Stuart, F. M.: The exhumation history of orogenic belts from 40Ar/39Ar ages of detrital micas, Mineralogical Magazine, 66, 121-135, 10.1180/0026461026610017, 2002.

Tetley, N., McDougall, I., and Heydegger, H. R.: Thermal neutron interferences in the 40Ar/39Ar dating technique, Journal of Geophysical Research: Solid Earth, 85, 7201-7205, https://doi.org/10.1029/JB085iB12p07201, 1980.

Turner, S., Sandiford, M., Flöttmann, T., and Foden, J.: Rb/Sr dating of differentiated cleavage from the upper Adelaidean metasediments at Hallett Cove, southern Adelaide fold belt, Journal of Structural Geology, 16, 1233-1241, https://doi.org/10.1016/0191-8141(94)90066-3, 1994.

Turner, S., Haines, P., Foster , D., Powell, R., Sandiford, M., and Offler, R.: Did the Delamerian Orogeny Start in the Neoproterozoic?, The Journal of Geology, 117, 575-583, 10.1086/600866, 2009.

Turner, S. P., Kelley, S. P., VandenBerg, A. H. M., Foden, J. D., Sandiford, M., and Flöttmann, T.: Source of the Lachlan fold belt flysch linked to convective removal of the lithospheric mantle and rapid exhumation of the Delamerian-Ross fold belt, Geology, 24, 941-944, 10.1130/0091-7613(1996)024<0941:sotlfb>2.3.co;2, 1996.

Wijbrans, J. R. and McDougall, I.: Metamorphic evolution of the Attic Cycladic Metamorphic Belt on Naxos (Cyclades, Greece) utilizing 40Ar/39Ar age spectrum measurements, Journal of Metamorphic Geology, 6, 571-594, https://doi.org/10.1111/j.1525-1314.1988.tb00441.x, 1988.

Zack, T. and Hogmalm, K. J.: Laser ablation Rb/Sr dating by online chemical separation of Rb and Sr in an oxygen-filled reaction cell, Chemical Geology, 437, 120-133, https://doi.org/10.1016/j.chemgeo.2016.05.027, 2016.